Technische Universität Berlin

Department of Chemistry

Synthesis and characterisation of calcium oxide catalysts for the oxidative coupling of methane (OCM)

Master Thesis

Prepared at: Fritz-Haber-Institut der Max-Planck-Gesellschaft

Submitted by: Lukas Thum

Submitted on: 14. July 2014

1. Examiner: Prof. Dr. R. Schomäcker

2. Examiner: Prof. Dr. R. Schlögl

Technische Universität Berlin

Institut für Chemie

Präparation und Charakterisierung von Calciumoxid-Katalysatoren für die oxidative Kupplung von Methan (OCM)

Masterarbeit

Durchgeführt am: Fritz-Haber-Institut der Max-Planck-Gesellschaft

Eingereicht von: Lukas Thum

Eingereicht am: 14. Juli 2014

1. Gutachter: Prof. Dr. R. Schomäcker

2. Gutachter: Prof. Dr. R. Schlögl

Die selbständige und eigenhändige Anfertigung versichert an Eides statt

Berlin, den

.....

Abstract

In this work pure calcium oxide was investigated as a model catalyst for the oxidative coupling of methane (OCM) and compared to magnesium oxide. For this purpose calcium oxide samples with diverse surface properties were synthesised, using different methods reported in the literature. For characterisation nitrogen adsorption (BET), (in-situ) X-ray diffraction (XRD), IR assisted CO adsorption, thermo-gravimetric analysis (TG) and electron microscope (EM) techniques were applied. Among the applied syntheses the Sol-Gel method produced the smallest particles and highest surface areas (up to $40\,m^2$). A microwave assisted hydrothermal method was successfully used to alter surface properties of calcium and magnesium oxide, reducing particle size, as well as increasing surface area. HR-TEM imaging proved the presence of monoatomic steps on both oxide surfaces. Using carbon monoxide as Probe molecule IR experiments were conducted, indicating multiple adsorption sites on calcium oxide. Due to the similarities in the IR patterns, the bands at $2154\,cm^{-1}$ were assigned to terrace sites and the band at $2164\,cm^{-1}$ to edge sites, according to literature data for magnesium oxide. Another absorption band $2141\,cm^{-1}$ was assumed to represent physisorbed carbon monoxide. An adsorption site relating to monoatomic steps, could, in case of calcium oxide, not be found. During catalytic testing (8 fold parallel reactor, 50 mg cat, N_2:CH_4:O_2 of 3:1:1, $47755\,h^{-1}$ GHSV) calcium oxide showed superior activity and selectivity (X_{CH4}: 25%, S_{C2}: 30%) compared to magnesium oxide(X_{CH4}: 8%, S_C2: 12%). Initial high activity could be linked to edge sites on the calcium oxide surface, which decreased in quantity due to sintering.

Zusammenfassung

In dieser Arbeit wurde reines Calciumoxid als Modellkatalysator für die oxidative Kupplung von Methan untersucht (OCM) und mit Magnesiumoxid verglichen. Dafür wurden, unter Verwendung von verschiedenen Methoden aus der Literatur, Calciumoxid-Proben mit unterschiedlichen Oberflächeneigenschaften hergestellt. Zur Charakterisierung wurden Stickstoffadsorption (BET), (in-situ) Röntgenstreuung (XRD), IR unterstützte CO Adsorption, thermogravimetrische Analyse (TG) und Elektronmikroskop (EM) Experimente durchgeführt. Von den verwendeten Synthesen produzierte die Sol-Gel Methode die kleinsten Partikel mit der größten Oberfläche (bis zu $40\,m^2$). Eine Mikrowellen unterstützte hydrothermal Methode wurde erfolgreich angewendet um die Oberflächenstrutur von Magnesiumoxid und Calciumoxid zu verändern, wodurch die Partikelgröße verringert und die Oberfläche um einen Faktor zwei erhöht werden konnte. HR-TEM Untersuchungen konnten die Anwesenheit von monoatomaren Stufen auf beiden Oxiden nachweisen. Mit Kohlenmonoxid als Sondenmolekül wurden IR Experimente durchgeführt, welche die Präsenz verschiedener Adsorptionszentren auf Calciumoxid zeigen konnte. Auf Grund von Ähnlichkeiten der IR Muster und Literatur-Daten für Magnesiumoxid, wurden die Banden bei $2154\,cm^{-1}$ Terrassen- und die Banden bei $2164\,cm^{-1}$ Kantenzentren zugeordnent. Eine weiteres IR Band bei $2141\,cm^{-1}$ wurde physisorbierten Kohlenstoffmonoxid zugeordnet. Ein Adsorptionszentrum, welches monoatomaren Stufen zugeordnet werden kann, konnte für Calciumoxid nicht gefunden werden. Während der Katalyse (8 fach parallel Reaktor, $50\,mg$ cat, N_2:CH_4:O_2 of 3:1:1, $47755\,h^{-1}$ GHSV) zeigte Calciumoxid eine überlegende Aktivität und Selektivität (X_{CH4}: 25%, S_{C2}: 30%) gengenüber Magnesiumoxid (X_{CH4}: 8%, S_{C2}: 12%). Die initial hohe Aktivität konnte mit den Kanten auf der Calciumoxid Oberfläche in Verbindung gebracht werden, welche auf Grund von Sinterung mit der Zeit abnehmen.

Acknowledgement

I would like to thank the staff of the FHI for the great support and help during my master thesis, especially

Dr. Annette Trunschke for the advice and supervision of this project,

Pierre Schwach for his shared knowledge and experience on this subject,

Jutta Kröhnert for help in matters concerning IR measurements,

Jasmin Allan and Frank Girgsdies for XRD and TG analysis,

Wiebke Frandsen for the nice electron microscope images as well as Dr. Thomas Lunkenbein and Dr. Marc Willinger for the HR-TEM images,

Maike Hashagen for BET measurements,

Dr. Johannes Noack for taking care of all the trouble with the microwave,

Olaf Timpe for organising equipment and help in the laboratory,

all other colleagues from reactivity group and all colleagues helping with measurements and the unfamiliar equipment.

Many thanks also to the staff of the FHI workshop and Carsten Hirschfeld of the TU Berlin for fast repairs and constructions.

I would also like to thank Dr. Thorsten Otremba and Dr. Frank Rosowski from the BasCat laboratory for conducting the OCM measurements.

Special thanks to my supervisors Prof. Robert Schlögl of the FHI and Prof. Reinhard Schomäcker of the TU Berlin for enabling this project as well as helpful advice.

Contents

1 Motivation

Failing to understand the role of the catalyst during the oxidative coupling of methane, new catalysts are designed by a bottom up approach, starting from simple metal oxides, while step wise increasing the complexity by doping and adding additional components. Using a single phase nonreducible materials with cubic structure, the number of present surface sites and thus potential catalytic active centres are manageable, allowing a systematic approach and isolation of the active species using various techniques like HAADF-STEM, HR-TEM, and adsorption techniques supported by computational studies.[1,2]

In case of MgO subsurface doping with transition metals can be successfully used to modify the electronic structure in favour of the catalytic performance. The fact, that the doping is subsurface, is important: transition metals on the surface may lead to unwanted redox reactions causing a combustion of methane and the OCM products.[3] Transition metals trapped inside an insulating oxide such as alkaline earth oxides, can donate electrons to adsorbates and hence promote a dissociative adsorption even on unreactive terrace sites.[4] By gold deposition, blocking steps on the catalyst surface, the sintering could be suppressed, creating a new more stable catalyst.[1]

For further improvement, instead of the magnesium oxide, the more active and selective calcium oxide can be used as new benchmark material. Recent studies showed evidence, that solid solutions of calcium oxide doped with Mo^{2+} exhibits favourable electronic properties for the methane activation.[4] An in-depth analysis of calcium oxide during the oxidative coupling of methane is therefore absolutely essential.

2 Introduction

2.1 Oxidative Coupling of Methane

The oxidative coupling of methane (OCM) was first introduced in the 80s,[5] which was a response to the strong price increases of crude oil, caused by middle east conflicts. New techniques and a new feedstock was needed in order to supply the chemical industry with basic chemicals.[6] One of the most important chemical compound is ethylene, being the source material for compounds such as polyethylene, dichlorethane, ethylene oxide, and so on. Produced by steam reforming of naphtha, the price for ethylene is directly linked to the oil price.[7]

The constant low natural gas prices made methane a suitable alternative to the established feedstock. In order to produce higher hydrocarbons out of methane, two molecules have to be coupled. By using oxygen as oxidising agent, hydrogen is eliminated forming water:

$$2CH_4 + \frac{1}{2}O_2 \rightarrow C_2H_6 + H_2O, \tag{1}$$

followed by a oxidative dehydrogenation:

$$C_2H_6 + \frac{1}{2}O_2 \rightarrow C_2H_4 + H_2O. \tag{2}$$

Given the strong C-H bond of methane (435 kJ/mol), due to its tetrahedral structure, high temperatures are needed in order to abstract hydrogen.[8]

Given the high temperature and the presence of oxygen and radicals in the gas phase, further oxidation is most likely, resulting in a product spectrum consisting of C_2-C_4 hydrocarbons as well as combustion products like CO and CO_2.

It is a widely accepted theory, that for the formation of the coupling product methyl radicals are are required,[9] where and how those are formed remained unclear.

In the early studies using Li promoted magnesium oxide as benchmark compound for kinetic investigations, Lunsford et al.[10] proposed a mechanism where [Li^+O^-] defect centres were responsible for the formation of methyl radicals:

$$Li^+O^- + CH_4 \rightarrow Li^+OH^- + \cdot CH_3, \tag{3}$$

in which those centres could be regenerated by water elimination in presence of oxygen:

$$2Li^+OH^- \rightarrow Li^+O^{2-} + Li^+\square + H_2O, \tag{4}$$

$$Li^+O^{2-} + Li^+\square + \frac{1}{2}O_2 \rightarrow 2Li^+O^-, \tag{5}$$

with $\square$ representing lattice vacancies.[10]

Years later it has been found, that independent from the preparation method, the lithium evaporates during the first hour on stream, proving this mechanism to be unlikely.[11] It is more likely, that the evaporation of the lithium creates defect sites on the surface instead of taking an actibe role in catalysis.[12]

Computational studies proved a decreased activation energy for the dissociative adsorption of methane on coordinative unsaturated surface sites compared to adsorption on terrace sites,[13,14] making these most likely to be the active centres for the OCM reaction. In figure 1 a proposed mechanism for the methyl radical formation on atomic steps on pure magnesium oxide is shown. In this mechanism methane is adsorbed on a Lewis acid/base pair located on a monoatimc step. There it can split forming a methanide anion and a hydroxyl group. The methanide anion is reduced by gas phase oxygen and desorbed as methyl radical, forming a superoxide species on the surface. The active site is aftwards regenerated by desorption of a perhydroxyl radical. EPR, IR as well as kinetic studies were applied to substantiate this concept.[2]

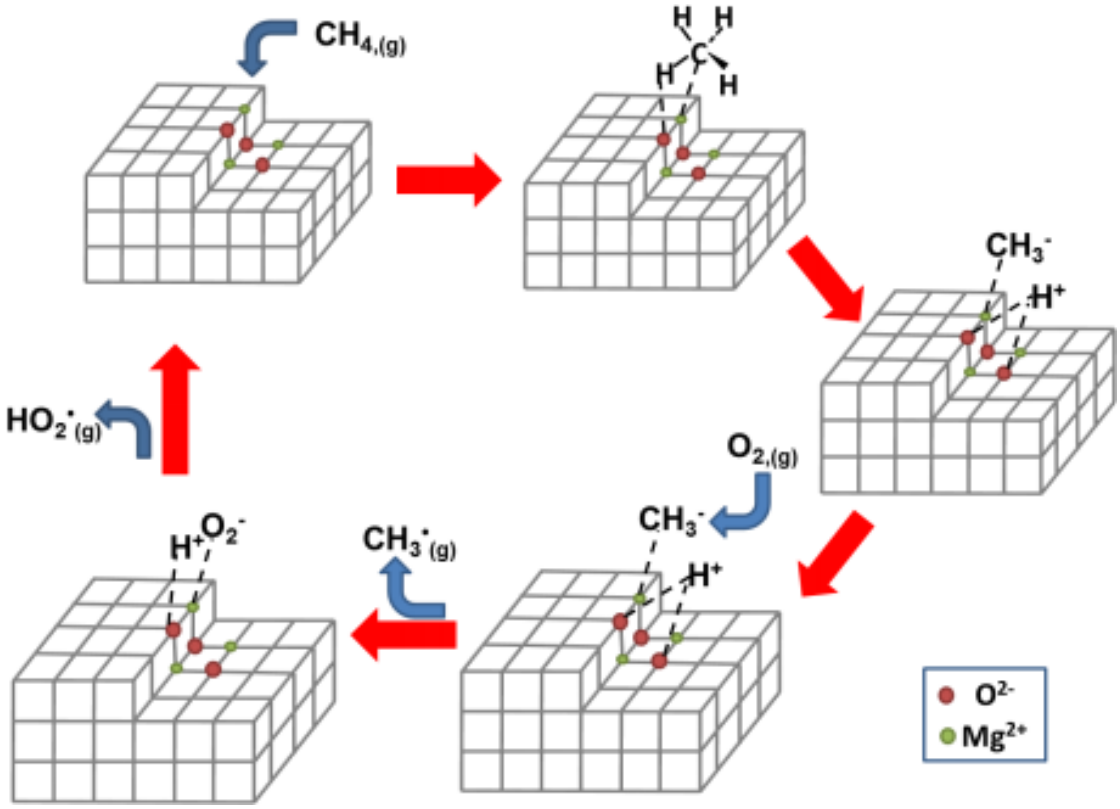

Figure 1: Proposed mechanism for methyl radical formation on pure MgO.[2]

2.2 Alkaline Earth Oxides in OCM

Since the early stages of the OCM research, alkaline earth oxides have been investigated for the use as catalyst. In terms of activity CaO proved to be the most active, followed by MgO and BaO, BeO and SrO. The best selectivity could be found for SrO and BaO, followed by CaO, MgO and BeO.[15–17] In general "good" performing catalyst found for the OCM reaction were of basic nature.[9] Due to the unfavourable chemical properties of SrO and BaO, like the thermal stability of the carbonates at reaction temperature,[18] and the toxicity of BeO, those materials were paid not as much attention compared to calcium oxide and magnesium oxide.

Numerous studies have been performed using alkaline earth oxides for the oxidative

coupling of methane, where in most cases doped oxides were investigated instead of the raw material. Most common doping agents used were lanthanide oxides and alkaline oxides[10,17,19–24]

Although redox active materials have been reported to promote the combustion of methane,[3,25] it is noteworthy that among the lanthanide oxides dopands even cerium oxide has proven to be beneficial to enhance the catalytic reactivity of methane.[21]

As for for alkali dopands lithium and sodium have proven to be most beneficial for the oxidative dehydrogenation of methane.[17,22,26] In case of sodium doped calcium oxide Lunsford et al.[19] suggested, in agreement with their prior studies on the lithium doped magnesium system,[10] $[Na^+O^-]$ centres to produce the needed methyl radicals (cf. section2.1). In recent theoretical studies Metiu et al.[14] supported this theory. Sodium dopands on the calcium oxide surfaces reduce the activation energy for the dissociation of methane. The sodium dopands are also more likely to be located at surface steps, where the activation energy is even lower. However it is also mentioned that the presence of O-H groups might nullify the promoting effect.[27] (Evidence for the presence of such groups can be found this project: section 4.3)

A selection of catalytic results of raw calcium oxide in the OCM reaction is presented in table 1. The catalytic activity among the catalysts differs quite strongly, with C_{2+} selectivities ranging from 8-55%. Though, due to the various applied reaction conditions, the comparability is limited. An et al.[28] suggested unsaturated surface sites to be the main reason for differences in the catalytic performance. It has been reported before, that those sites have an enhanced ability to activate oxygen, making them active for reactions involving oxygen.[29,30] Given the different applied synthesis routes, differences in the surface site composition are highly likeable.

A problem for all calcium oxide based catalyst is the sintering. Sintering of pure calcium oxide at high temperatures is unavoidable.[31] Under reaction or preparation conditions this effect can be strongly enhanced by the presence of H_2O and CO_2,[32] both by-products

Table 1: Catalytical properties of CaO reported in the literature.

Source material	Synthesis method	BET surface [m^2/g]	W/F [$g \cdot s/ml$]	S_{C2+} [nm]	X_{O2} [%]	Feed inert:CH_4:O_2	T [°C]
$CaCO_3$ [16]	pellet	7,6	0,17	47	100	1,3:3,3:4,0	740
$Ca(OH)_2$ [16]	powder	6,3	0,13	55	94	1,3:3,3:4,0	740
$Ca(OH)_2$ [16]	pellet	5,6	0,71	46	94	1,3:3,3:4,0	740
$Ca(OH)_2$ [17]	pellet	n.a.	0,1	55	94	13,0:33,5:3,9	740
$Ca(OAc)_2$ [21]	powder	5,4	0,07	33	n.a.	0:8:1	800
$Ca(OAc)_2$ [22]	powder	6,0	0,7	49	n.a.	0:4:1	750
$Ca(NO_3)_2$ [28]	powder	18,8	0,6	50	n.a.	10:8:2	750
$Ca(OH)_2$ [15]	powder	18,8	n.a.	46	100	0:5:1	750
CaO [19]	commercial	6	0,87	8,2	n.a.	647:76:37	700

of the OCM reaction, which leads to an auto-poisoning of the catalyst and a steady state analysis quite difficult.

Attempts have been made to stabilise the catalysts and decrease the deactivation rate. Coating silica with calcium oxide has proven to improve the stability, in respect to the surface area and the selectivity, implying a enhanced stability for unsaturated surface sites.[28] Another attempt has been made to thermally stabilise CaO, by deposing it on MgO nanoparticles.[33,34] Not having performed catalytic test with those compounds, the stability to H_2O and CO_2 atmosphere however, has yet to be proven. Known to form Mg-Ca-O mixed phases at the interface, the catalytic performance might also be altered.

2.3 Surface Probing Using CO

As mentioned above the surface site composition has a huge effect on the catalytic performance. Therefore a method for surface site characterisation is needed in order to make founded assumptions on catalytic centres. An established method to investigate surfaces is the adsorption of IR active probe molecules on the surface. A common molecule for probing basic surfaces is carbon monoxide. An extensive review about CO interactions with different surface site was published by Hadjiivanov and Vayssilov.[45] A review about CO adsorbed on MgO surfaces was published Zecchina et al.[35] summarising 30 years of data on this matter.

Adsorbing CO at low temperature on magnesium oxide, the adsorption can take place in a non-reactive manner, where the CO is bound to the cation center. The adsorbtion leads to a positive shift in the C-O stretching mode (2143 cm^{-1}), in which the strength of the shift is affected by the coordination state of the cation and can be detected by IR-measurements. The strength of polarising field of the cation directs the strength of the shift. Less saturated sites exhibit a stronger positive field and thus result in a stronger shift of the C-O stretching mode.

Adsorbtion experiments with accompanying HR-TEM imaging made a profound assignment of the resulting bands possible. By investigating pristine MgO cubes with increasing particle sizes, the ratio of corners to edges to terrace sites could be observed and compared to the resulting IR spectra.

The most unsaturated corner sites (Mg^{2+}_{3C}) were assigned to bands at 2205-2200 cm^{-1}. For the edge sites (Mg^{2+}_{4C}) two different sites could be observed. The sites more present on more sintered samples were assigned to multiatomic edge sites at 2180-2160 cm^{-1} and the ones more abundant on non-sintered magnesium oxide at 2150-2145 cm^{-1} to step sites. The weak shift of the step bound site and yet strong adsorption enthalpy led to the assumption, that the CO in this case is adsorbed is of different nature compared

to the other sites. There are a few possibilities discussed in the literature (figure 2) how CO is bonded to the MgO surface. All theories agree on the involvement of two

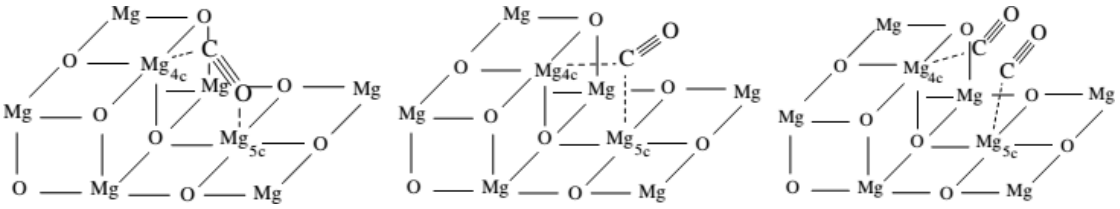

Figure 2: Proposed adsorption for CO on steps on MgO[35].

sites, explaining the strong adsorption enthalpy. The last species at 2157-2149 cm^{-1} was assigned to terrace sites (Mg^{2+}_{5C}).

A different type of species formed during the adsorption, by CO adsorbed on unsaturated O^{2-} sites, are the carbonites (CO_2^{2-}). Due to the formation of poly-structures, the resulting IR spectra are complex and hard to interpret, making the bonds between 2000-1000 cm^{-1} unfavourable for surface analysis.

Due to the fact, that no research could be found that identifies the surface sites on calcium oxide, the studies conducted magnesium oxide are the closest to compare to for getting insights on the surface composition. A certain similarity between in the adsorption behaviour of both oxides could be found by Babaeva et al.,[36] making this a valid approach.

3 Aim of the Master Thesis

The aim of this project is the investigation of the suitability of calcium oxide as a new benchmark material for further OCM research, replacing the not so successful magnesium oxide catalysts. Therefore pure calcium oxide samples have to be tested in the OCM and analysed.

Of special interest is the influence of the surface structure on the catalytic performance. For this purpose a variety of calcium oxide samples will be prepared using different methods reported in the literature, developing unique surface site compositions.

In order to observe the different surface sites, the samples will be investigated using CO adsorption experiments, coupled with IR measurements. Given the lack of reference data for calcium oxide, the results will be compared to adsorption experiments on magnesium oxide, verifying whether this technique is suitable for calcium oxide as well.

The surface properties of the calcium oxide samples will further be analysed using electron microscopy, X-ray diffraction and nitrogen adsorption methods.

4 Results and Discussion

4.1 Catalyst Preparation

A selection of syntheses reported in the literature were applied to obtain calcium oxide samples with diverse surface properties: a precipitation method [37], where calcium nitrate was precipitated using sodium hydroxide, a citrate method [38,39], where calcium was embedded in a combustible organic matrix and a Sol-Gel inspired method [40], where calcium methoxide was formed by reacting metallic calcium with methanol followed by hydrolysis. A microwave assisted hydrothermal method was used on existing oxides, altering the surface sites. [1] The catalyst were calcined at a temperature of 850 ° for at least 6 hours. The high temperature was chosen to ensure in the complete decomposition of the precursor materials. The procedures were selected based on promising product properties as well as the availability of high grade source materials. An accurate description of the procedures can be found in section 7.1.

4.1.1 Hydrothermal Treatment

The first approach to create oxides with new surface properties was the microwave assisted hydrothermal treatment. Commercial bought oxides were hydrolysed with water in a microwave autoclave to the corresponding hydroxide and afterwards calcined to the oxide. The cheaper magnesium oxide was used to optimise the procedure by varying temperature as well as duration of the process. Two different autoclave systems were tested: a stirred one and an unstirred one. The samples were analysed with nitrogen adsorption (surface area), XRD analysis (particle size using Scherrer method) and electron microscopy (morphology). The results can be found in table 2.

From the varied parameters the stirring had the most influence on the resulting product, achieving the biggest boost in surface area. Variation of the temperature and the

Table 2: Properties of hydrothermal treated MgO and CaO in microwave autoclaves.

Material	Sample ID	Synthesis	BET surface [m^2/g]	Particle size [nm]
MgO	16796	C-MgO	49,7	22
MgO	16801	unstirred, 200°C, 180 mins	83,4	22
MgO	16894	unstirred, 220°C, 30 mins	87,6	21
MgO	17013	stirred, 200°C, 45 mins	81,6	24
MgO	17014	stirred, 200°C, 45 mins	90,6	22
MgO	17480	stirred, 180°C, 45 mins	102,6	19
CaO	17386	C-CaO	4,5	87
CaO	17492	stirred, 180°C, 45 mins	9,0	50

synthesis time had no strong effect. The TEM images (figure 3) show that after calcination the former isolated MgO cubes form a hexagonal superstructure. This structure is a remnant of the hexagonal structure of the hydroxide. Whereas in both cases the size and roughness of the MgO cubes seem to be similar, the hexagonal platelets in the stirred system are much thinner compared to the unstirred microwave system resulting in higher surface areas.

Using the optimal conditions found with the magnesium samples, calcium oxide samples were prepared. The surface area as well as particle size could be enhanced as well, but due to the much larger particles of the raw material compared to the magnesium oxide, the surface area of the product is low as well.

In figure 4 SEM images of the commercial CaO and an exemplary product of the applied procedure are shown. In agreement with the results of the magnesium samples, calcium oxides also form a hexagonal platelets according to the hydroxide structure.

The microwave assisted hydrothermal treatment can be used to alter the surface of the investigated oxides causing a decrease of the particle size as well as an increase of the

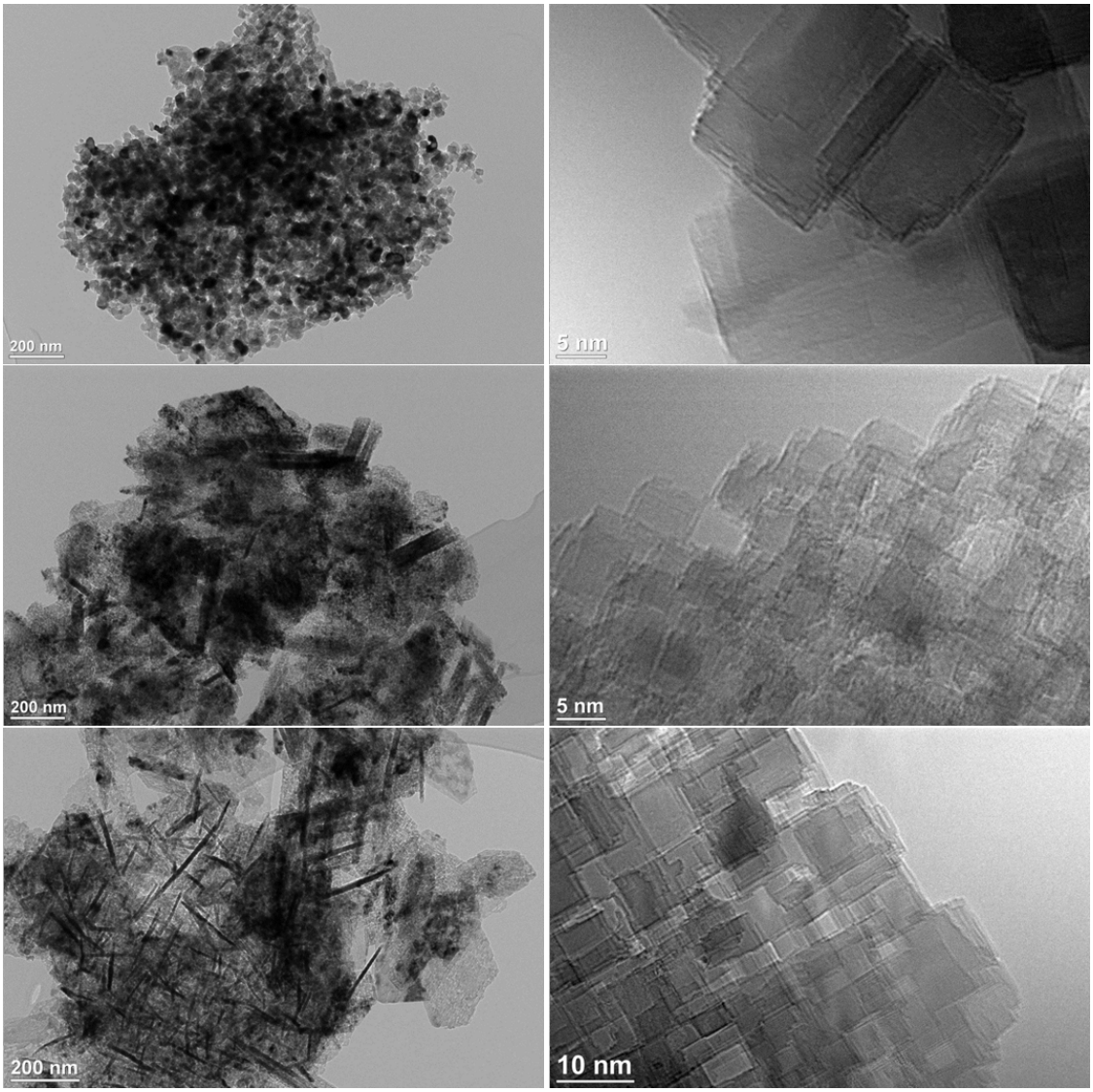

Figure 3: TEM images of hydrothermal treated MgO samples. Commercial MgO (top, 16796), MgO using unstirred microwave autoclave (middle, 17138 same synthesis as 16801) and MgO using stirred microwave autoclave (bottom, 17480).

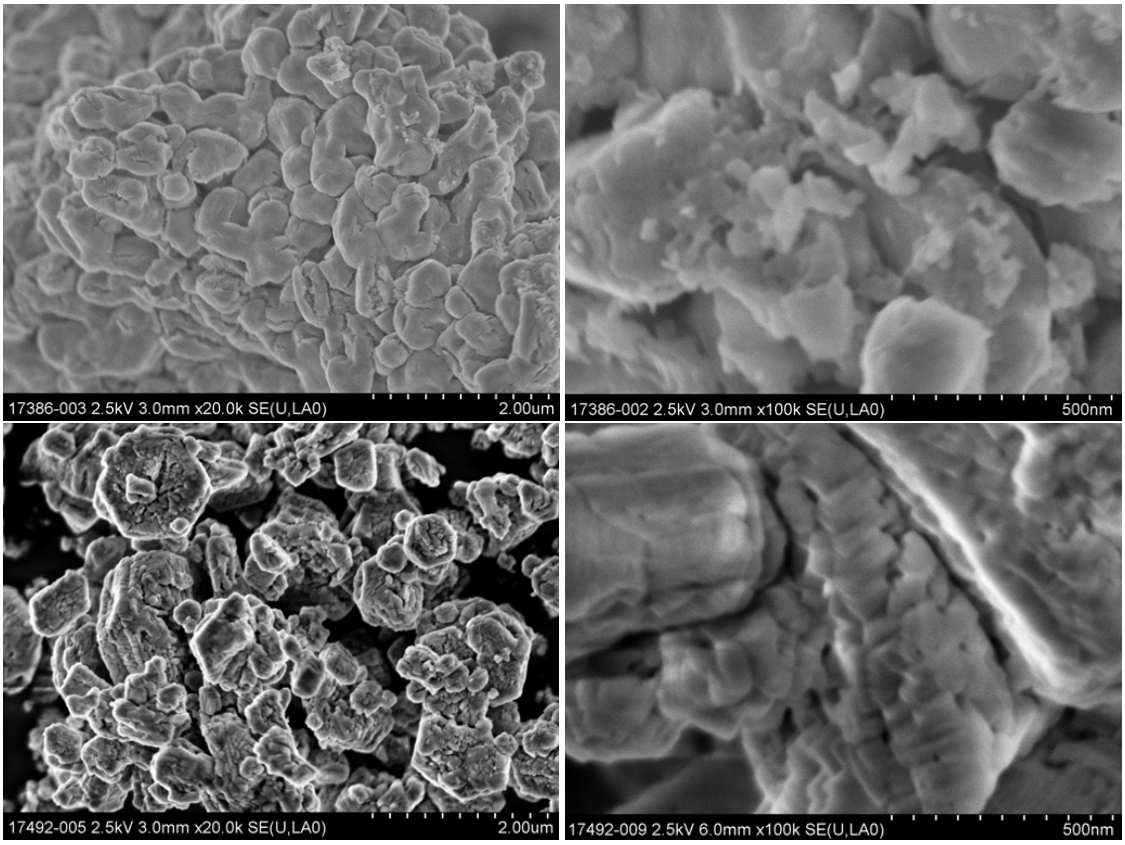

Figure 4: SEM images of commercial CaO (top, 17239) and hydrothermal treated CaO (bottom, 17492).

surface area by a factor two. With only using water as reagent, embedding of impurities is unlikely.

4.1.2 CaO Synthesis

The low surface area of commercial calcium oxide prevented a successful analysis using CO adsorption, therefore the oxides had to be synthesised.

4.1.2.1 Precipitation Method

The idea of the synthesis was to precipitate calcium nitrate with sodium hydroxide and age the particles using a microwave system, which should result in monodisperse particles with a surface area of $70\,m^2/g$.[37] The described procedure could not be reproduced. TEM images (figure 5) of an exemplary sample using this procedure show ill defined

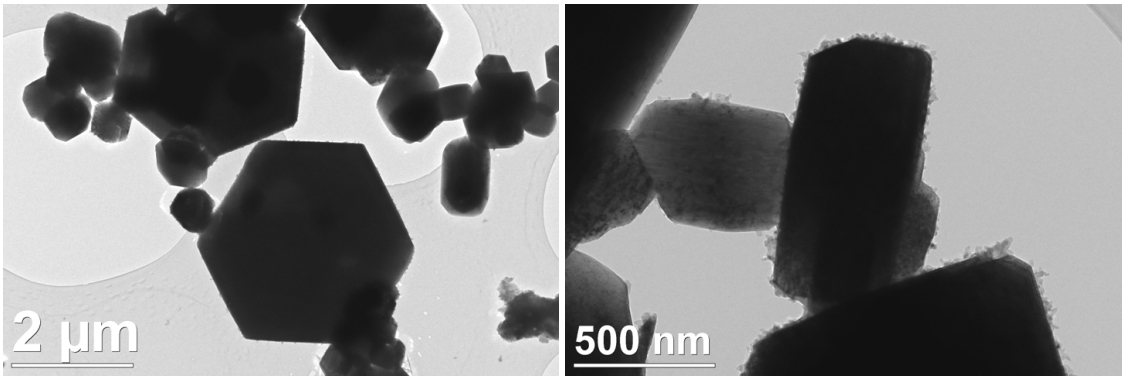

Figure 5: TEM images of CaO synthesised via precipitation method (17582).

non-uniform particles (further analysis was dropped).

Due to the product being far shown the results presented in the literature and the fact that alkaline impurities are well known to enhance the catalytic activity,[14,19,24,25,41] this procedure was eliminated from further investigations.

4.1.2.2 Citrate Method (citrate-)

By evaporating the water from a solution of citric acid and calcium nitrate a sticky yellowish gel is formed, which decomposes at 393 K, making a complete drying challenging. Decomposing this, a spongelike structure consisting of cuboid terraces is formed (figure 6) with a surface area of 20-30 m^2/g (literature 12 m^2/g and 45 m^2/g).[38,39]

In the thermal analysis multiple combustion steps could be observed, making a controlled stepwise decomposition almost impossible (figure 7). It can be noted, that the presence of oxygen is needed to fully convert the precursor into the oxide.

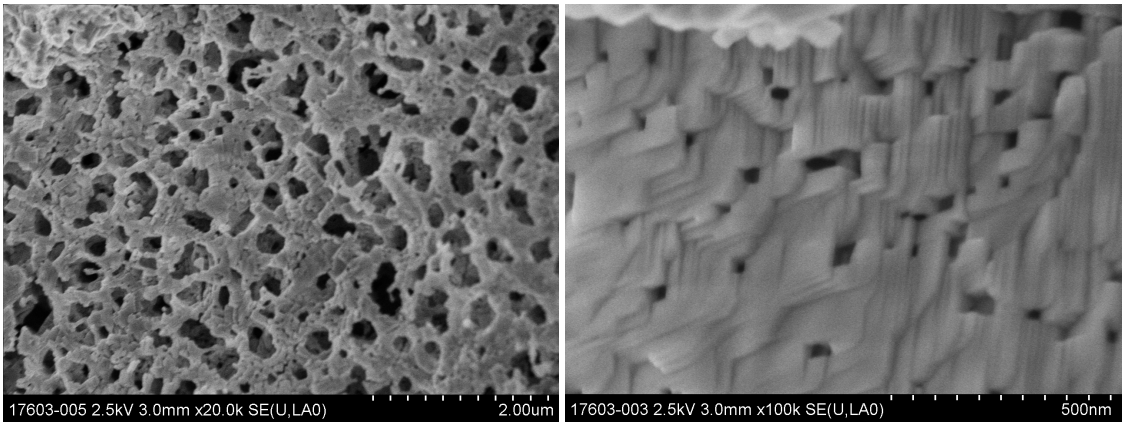

Figure 6: SEM images of citrate-CaO (17603).

A mass loss of over 80% while producing all kind of hydrocarbons and NO_X compounds making this procedure pretty nasty.

The high carbon content and the uncontrolled decomposition makes an embedding of carbonate and carbide into the calcium oxide structure possible. This might lead to an impure structure and might be considered in further discussions concerning reactivity and CO-adsorption experiments.

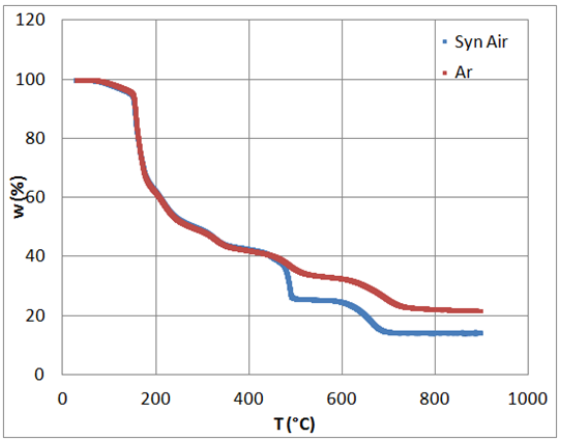

Figure 7: Weight loss of citrate precursor (17623) during calcination in argon and synthetic air.

4.1.2.3 Sol-Gel Method (SG-)

In an usual Sol-Gel procedure a metal alkoxide solution is hydrolysed by slowly adding water forming a sol, which through aggregation slowly becomes a gel. By drying the gel at high temperatures (538 K) and pressures (40 bar) using an autoclave the gel can be transform into an aerogel resulting in well dispersed high surface area oxides.[40,42]

However, in this case calcium and methanol form an insoluble solid under hydrogen evolution, which is not easily hydrolysed by adding water. Instead a quite stable compound is formed, which is used as catalyst for transesterification reactions.[43] The higher stability of the calcium methoxide compared to the magnesium methoxide, which is easily hydrolysed,[44] might be beneficial for the dissociation of methane during the OCM reaction. Nevertheless, the resulting compound can be calcined to the wanted oxide. Figure 8 shows the IR-spectra of the precursor and the oxide activated inside the IR set-up.

The IR spectrum of the precursor shows the presence of O-H groups (3600-3700 cm^{-1}), C-H stretching (2800-3000 cm^{-1}), -C-H bending (1460 cm^{-1}), -C-O primary alcohol stretching (1050-1085 cm^{-1}) as well as adsorbed CO_2 (1300-1800 cm^{-1}).[43] The presence of mul-

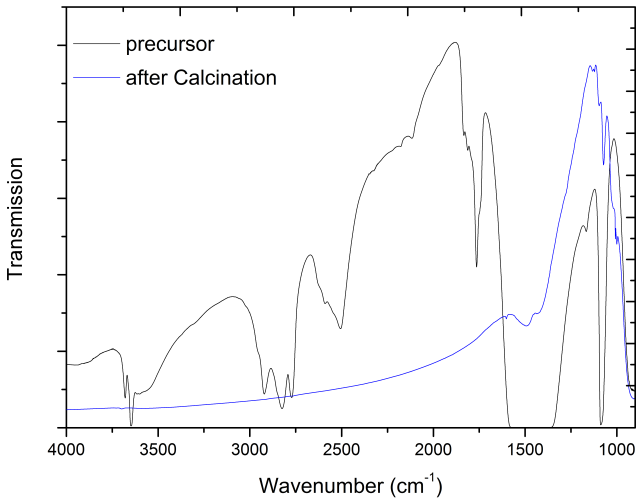

Figure 8: IR-spectra of SG-precursor (17912) before and after vacuum activation.

tiple species of O-H groups indicate a partial hydrolysis of the product. Despite being able to fully hydrolyse the methoxide, adding water appears to have an beneficial effect for the resulting precursor. In a test where the methoxide-toluene solution was split and one part was treated with water and the other not, the sample treated with water produced a precursor with a superior surface area (92,7 m^2/g) compared to the sample not treated with water (77,6 m^2/g). Figure 9 shows SEM images of the precursor and the calcined oxide displaying a foliaceous structure for the precursor, and large particles after calcination. The size of the cuboid like particles varies strongly between small particles with a size of about 50 nm up to a size of 250 nm. After calcination the superstructure of the precursor is almost lost, indicating a strong sintering during calcination.

The thermal analysis shows a two step decomposition of the precursor (figure 10) with an overall weightloss of 25%.

Given that the presence of H_2O and CO_2 accelerates the particle growth of CaO,[32] a step wise decomposition at 673 K, 873 K and 1123 K was used to improve the synthesis,

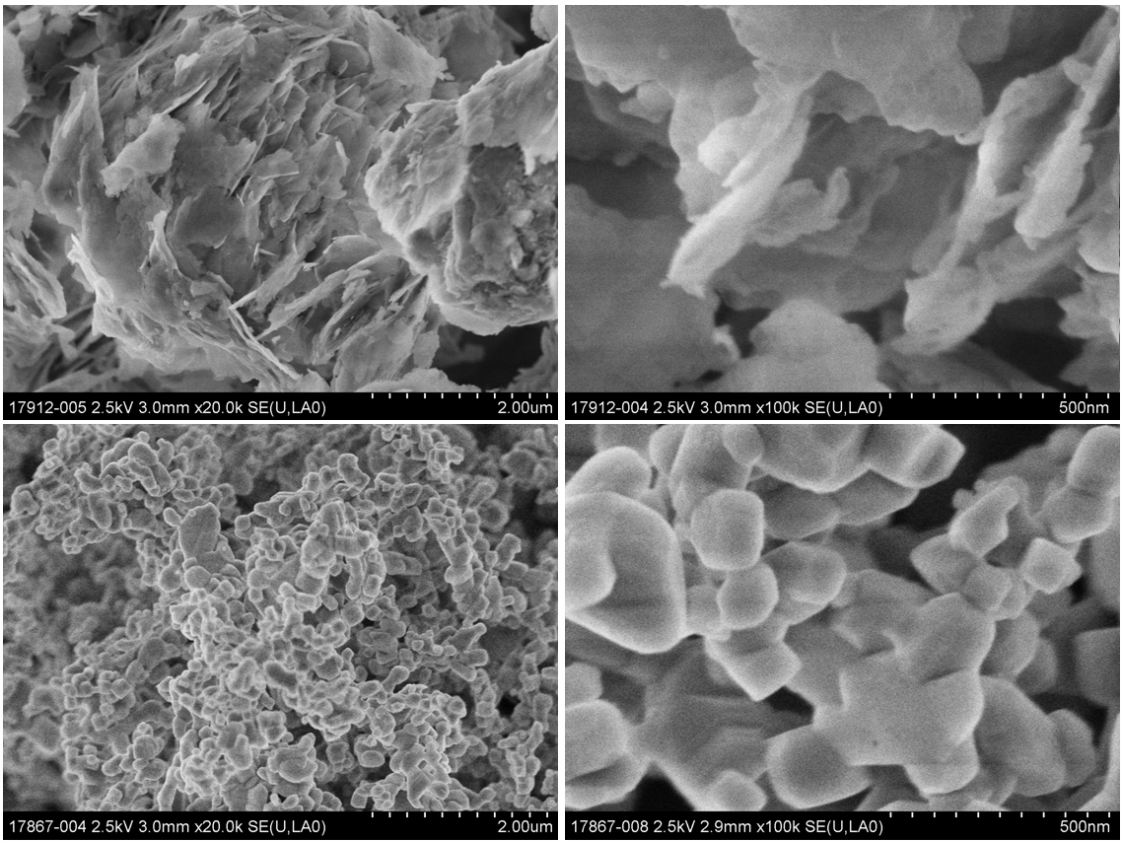

Figure 9: SEM images of SG-CaO. Before calcination (top, 17912) and after calcination (bottom, 17867).

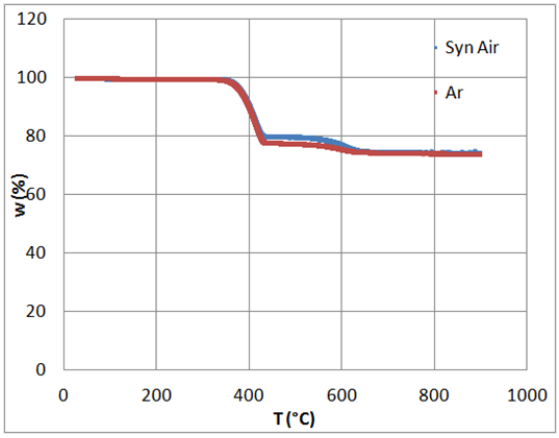

Figure 10: Weight loss of Sol-Gel precursor (17805) during calcination in argon and synthetic air.

as well as a synthesis under dynamic vacuum. SEM images (figure 11) prove a decrease of the particle size for both cases and also show the still intact precursor superstructure in case of vacuum calcination. This time the particle size distribution appears to be more uniform compared the first sample.

Without applying vacuum during calcination calcium oxide samples could be produced with a surface area of up to $40\,m^2/g$ (literature: $35\,m^2/g$, $140\,m^2/g$ applying vacuum, max calcination temperature $773\,K$) [40].

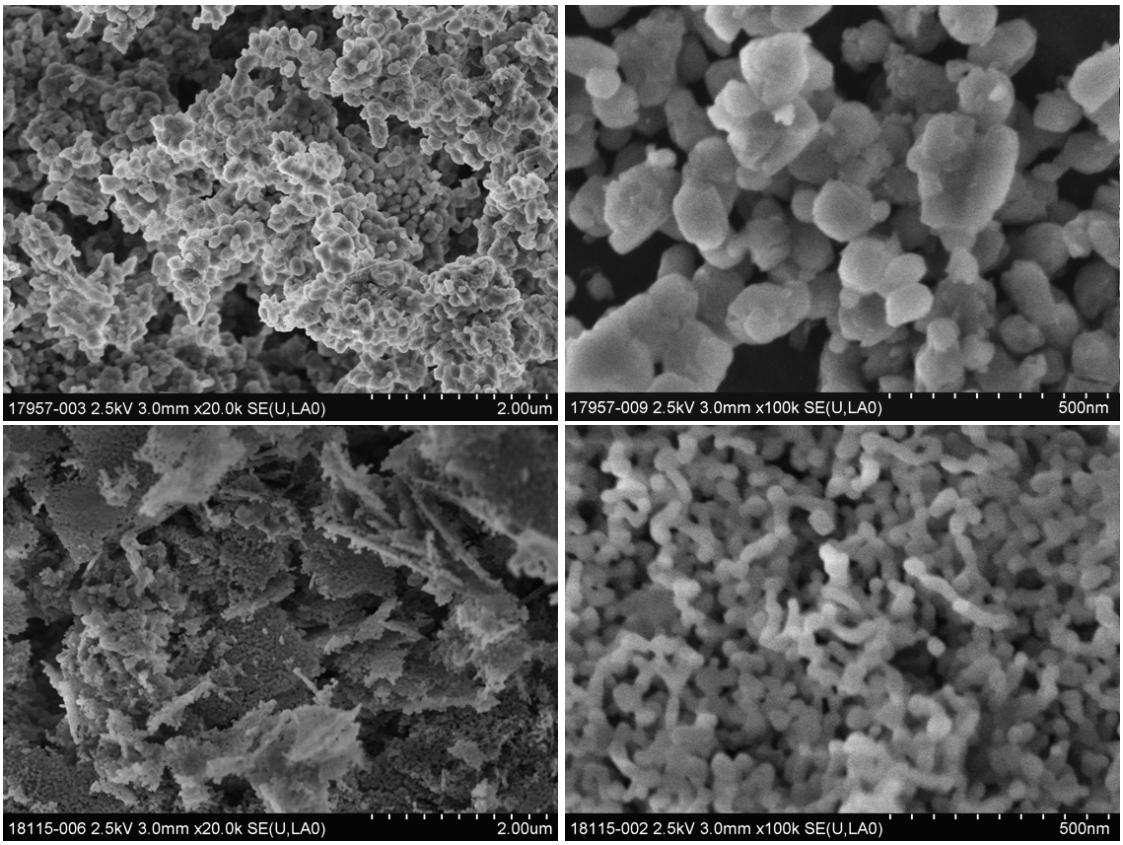

Figure 11: SEM images of SG-CaO after calcination using temperature ramp (top, 17957) and in vacuum (bottom, 18115).

4.2 General

The resulting surface areas for the calcium oxide samples reached from 9-40 m^2/g and 50-120 m^2/g for magnesium oxide. The best results calcium oxide could be achieved using the Sol-Gel method, followed by the citrate method. The most crucial part of the synthesis appears to be the calcination process. The particle growth during the calcination is strongly affected by the present gases. Gases that tend to react with alkaline earth oxide like CO, CO_2 and H_2O have to be avoided in order to achieve small particles with high surface areas. Therefore a calcination in vacuum will achieve the best results. Starting for organic components like calcium methoxide or the citrate precursor a calcination in absence of oxygen however might favour an incorporation of carbon in the product. Therefore all calcinations for the catalysts were performed in a synthetic air stream. Due to the ill shaped nature and the high possibility of alkaline impurities the precipitated samples, none of those were used for catalytic testing. In contact with air, calcium oxide quickly reacts to the hydroxide. However, due to the insulating properties and thereby strong electrostatic charging a sample preparation for IR or OCM experiments inside a glove box could not be realised. Therefore the formed hydroxide were in-situ reactivated prior to all other experiments.

4.3 IR-Investigation

Comparing raw IR-spectra of magnesium oxide and calcium oxide (figure 12), traces of carbonate can be found (1250-1600 cm^{-1}), which might be adsorbed during sample preparation and afterwards trapped inside the oxide during the calcination process. In contrast to MgO, CaO shows indications of O-H terminations on the surface (3650-3750 cm^{-1}) in spite of the heat treatment at 1123 K, proving its more basic nature.

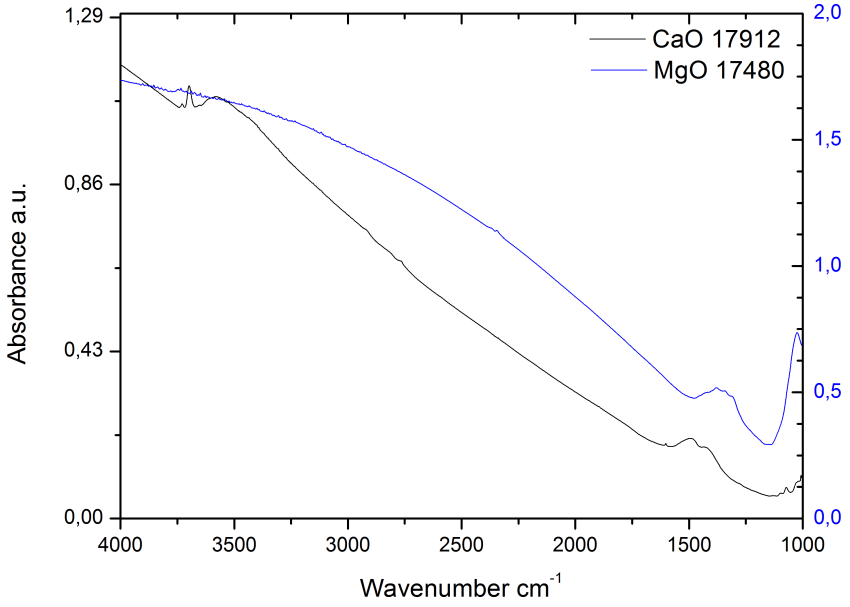

Figure 12: IR-spectra at 77K of MgO (17480) and CaO (17912).

4.3.1 CO-Adsorption

Adsorbing CO at low temperatures can result in a reversible adsorption of CO on coordinatively unsaturated metallic centres, such as M^{2+}_{3C} (corner site), M^{2+}_{4C} (edge site), M^{2+}_{5C} (terrace site), or in an irreversible reaction forming compounds like carbonites and carbonates. Basic materials like CaO and MgO can weakly adsorb CO resulting in a slightly positive shift in the stretching mode of the free CO molecule ($2143\,cm^{-1}$), in which the shift depends on the saturation of coordination sphere. The shift is the strongest for highly unsaturated sites like corners and weakens with the saturation.[36,45]

Due to the lack of data in the literature concerning CO adsorption on CaO at 77 K, MgO was analysed as well in order to find similarities.

In presence of helium for heat transfer CO was progressively adsorbed at 77 K on the oxide surface. A spectrum of the raw corresponding oxide sample was subtracted from the acquired spectra giving the absorption difference. This was done in order to investigate

the influence of the CO on the resulting spectra. Prior to the adsorption experiment the samples were activated at 1123 K for 6 hours. The spectra of the full observed area is shown in figure 13. Three areas in the spectra can be observed, which are influenced

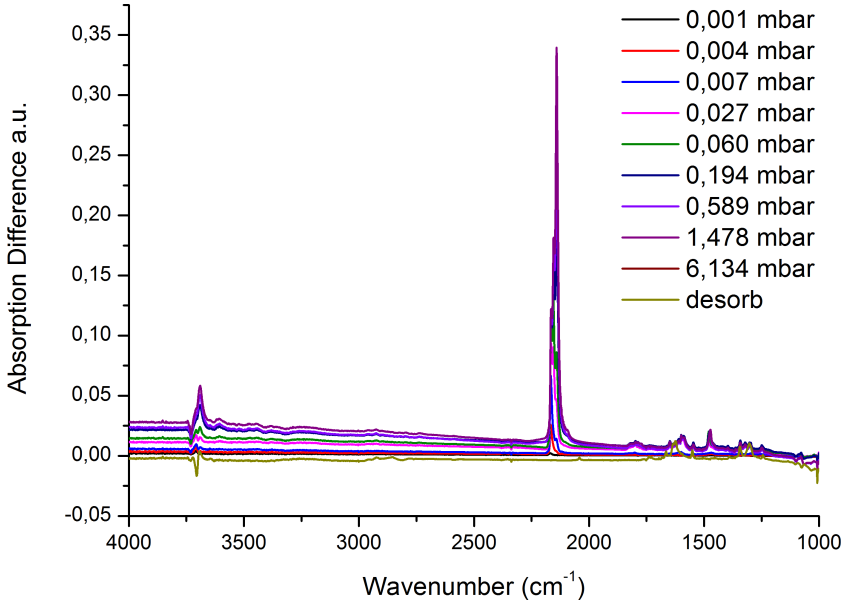

Figure 13: Full IR-spectra at 77K of CaO (17912) during CO-adsorption experiment.

by the CO dosage: at 1000-2000 cm^{-1} representing formed carbonite species, at 2100-2200 cm^{-1} representing adsorbed carbonyl species and at 3600-3700 cm^{-1} representing O-H species.

In figure 14 the IR spectra in the carbonyl area (2100-2200 cm^{-1}) during the CO adsorption experiment are presented. For both oxides it can be observed, that the bands at higher wave numbers evolve first at low CO pressures and are fast saturated, indicating only a small amount of the corresponding surface site and a higher heat of adsorption. With increasing pressure the peaks at lower wave numbers evolve until a saturation is reached and the signal corresponding to free CO molecules at 2143 cm^{-1} becomes dominant. After degassing and desorbing (MgO brown curve, CaO dark green) two species at lower wave numbers (MgO 2146 cm^{-1}, CaO 2141 cm^{-1}) are harder to desorb than the other species. Indicating the presence of a strongly linked CO molecule.

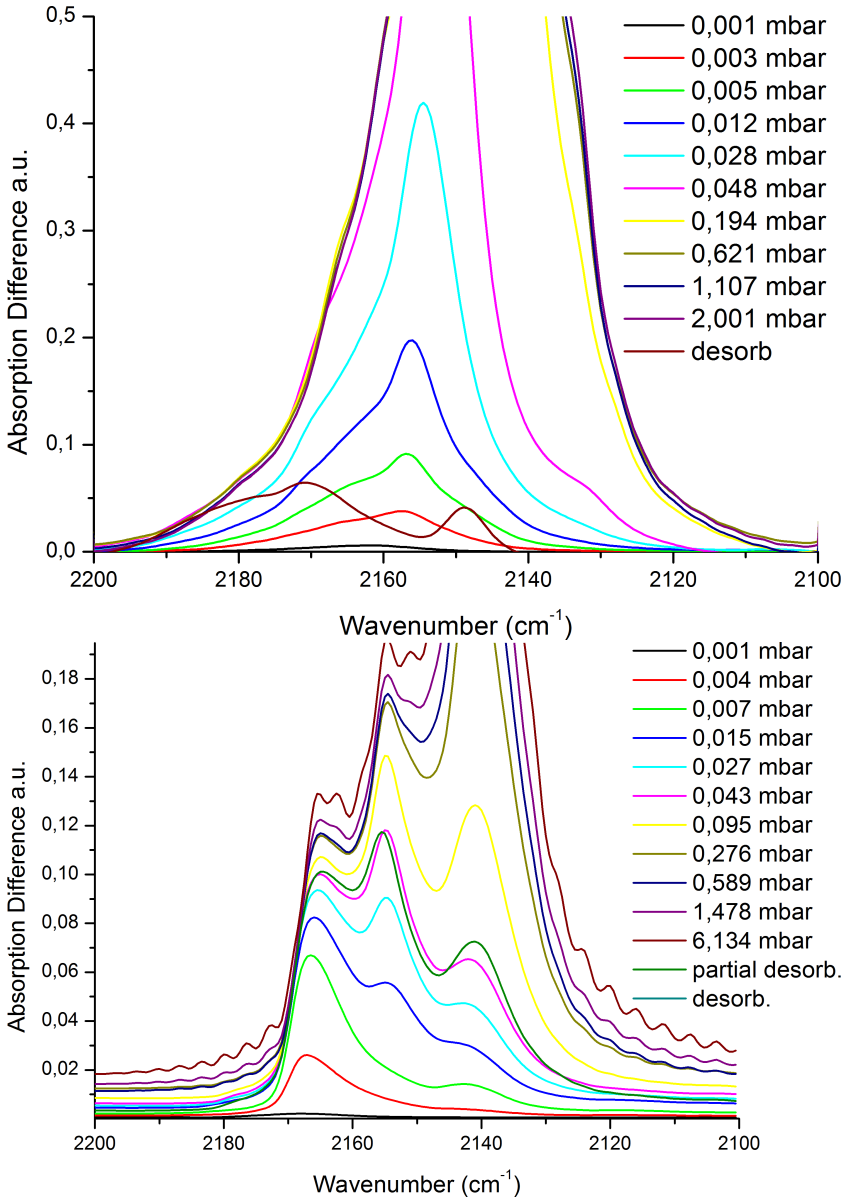

Figure 14: IR-spectra at 77K of MgO (top, 17480) and CaO (bottom, 17912) during CO-adsorption experiment.

The carbonite area (1000-2000 cm^{-1}) is shown in figure 15, exhibiting only a negligible amount of carbonites for both materials. In contrast to the adsorbed carbonyl species,

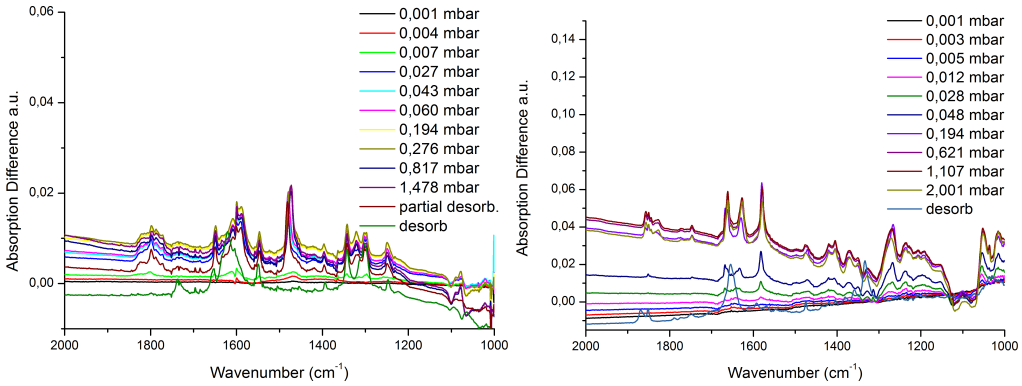

Figure 15: Carbonite area of IR-spectra at 77K of MgO (left, 17480) and CaO (right, 17912) during CO-adsorption experiment.

the carbonite species is already saturated at low CO pressures, whereas the carbonyl bond slowly evolves presenting multiple distinct adsorption species. It has to be mentioned, that the carbonite species do not fully desorb while degassing, makning this an irreversible process.

Due to the lower surface area of the CaO sample and the resulting adsorption capacity, the surface is saturated more quickly and rotational vibrations can be observed from the free CO molecules.

The positions of the carbonyl bands on MgO were discussed by Spoto et al.[46] assigning bands located between 2149-2157 cm^{-1} to terrace sites, 2160-2180 cm^{-1} to edge sites and 2200-2205 cm^{-1} to corner sites. Due to the low concentrations of corners, they could not be observed.[36] After partial desorption of CO another species becomes visible at 2146 cm^{-1}, which can be assigned to a CO molecule bonded to multiple atoms on atomic steps[46]. Another possibility was presented by Trionfetti et al.[47] assigning the signal to a CO molecule coordinated at the edge of an atomic step and a terrace site below.

To compare the IR spectra of MgO with CaO, a coverage was calculated by plotting the integrated carbonyl area (A) (using Origin 8.5 pro) of the IR spectra vs. the CO pressure (figure 16). Assuming a monolayer of CO is reached when the sample is fully saturated with CO and the integrated peak areas are constant, the coverage was calculated by

$$\Theta = \frac{A}{A_{sat}}.$$

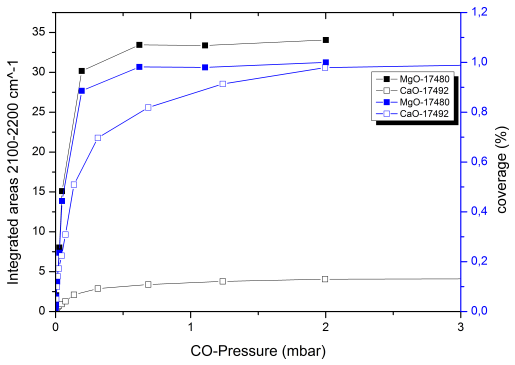

Figure 16: CO-coverage and integrated carbonyl peaks vs. CO pressure.

Figure 17 shows the IR spectra of the carbonyl area at a coverage of approximately 23%. The adsorption pattern of CO on CaO resembles the pattern on the MgO sample with

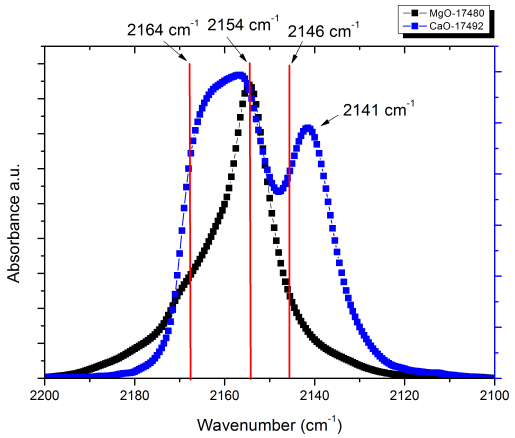

Figure 17: Carbonyl area at approximately 23% CO coverage at 77K of CaO and MgO.

exception of the peak at 2141 cm^{-1}. Due to the similarity with the free CO molecule and the absence of rotational frequencies, this might be physisorbed CO. Given the similarity between the two compounds and the intensity distribution, it can be assumed that the more intense peak at 2154 cm^{-1} represents terrace sites and the peak at 2164 cm^{-1} edge sites. Considering the intensity proportions for the adsorption sites, it can be noted, that ratio of terrace to edge sites on the magnesium sample is much higher compared to the calcium sample. In figure 18 HR-TEM images of a magnesium oxide and a calcium oxide sample (comparable to the samples used for the IT experiment) are presented supporting this assumption. The magnesium oxide sample exhibits mostly terrace sites, whereas the calcium oxide surface appears to be more rough exhibiting a multitude of edges. In both cases a few monoatomic steps can be observed, whereas an indication for monoatomic steps on CaO on during the IR-experiments could not be evidently observed.

Except for the presence of the three observed peaks during this experiment[36], there is also nothing reported in the literature on this subject.

Observing the O-H area (3600-3700 cm^{-1}) during the CO adsorption experiment (figure 19) it can be noted, that during the experiment there is a shift, which is only partly reversible. It can be assumed that the hydrogen terminations interact with CO from the gas phase (reversible part) and the formed carbonite species (irreversible part).

In summary CO adsorption has proven to be a powerful tool to analyse surface properties of both oxides. The IR pattern of MgO and CaO resemble each other allowing a founded assignment for the IR bands to the corresponding adsorption sites. Though a slightly stronger bound CO species can be observed at 2141 cm^{-1}, it would be highly speculative to assign this peak to monoatomic steps.

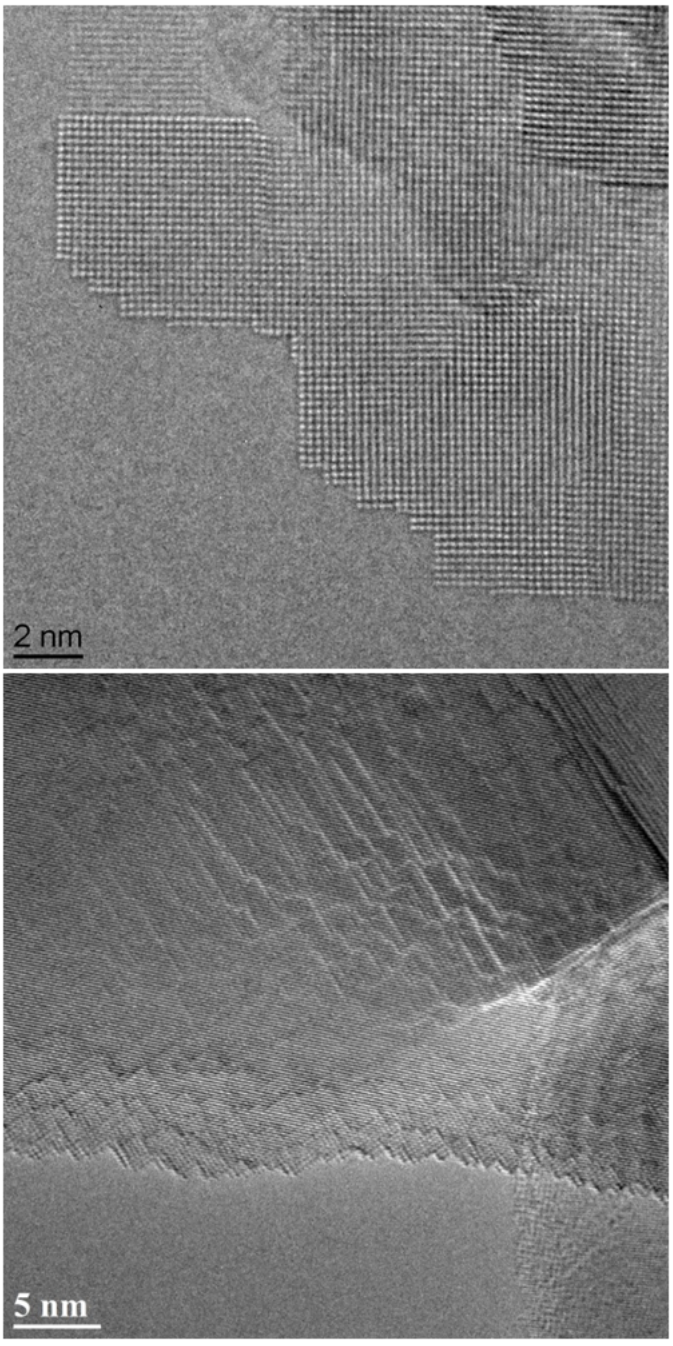

Figure 18: HR-TEM images of MgO (17480, top) and CaO (18115, bottom).

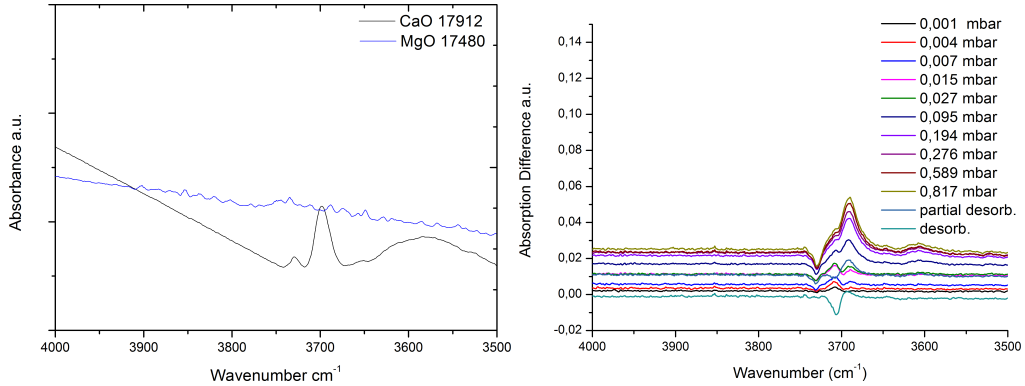

Figure 19: OH area of IR-spectra at 77 K (left) of MgO (17480) and CaO (17912). OH area during CO-adsorption experiment (right).

4.4 Catalysis

For the catalytic studies four calcium oxide samples prepared by different synthesis techniques, and two magnesium oxide samples were used. The calcium oxide samples were synthesised by Sol-Gel method, by the citrate method and the raw commercial CaO was used. For magnesium oxide the raw commercial one and a hydrothermal treated oxide were used. The surface areas of the catalysts can be found in table 3.

Table 3: Properties of MgO and CaO samples used in catalytic tests.

Material	Sample ID	Synthesis	BET surface $[m^2/g]$
CaO-C	17239	commercial	11,1
CaO-SG	18227	SG	33,8
CaO-SG-ramp	18228	SG, ramped calcination	39,9
CaO-citrate	18320	citrate C	32,1
MgO-C	16795	commercial	57,2
MgO-MW	17585	unstirred, 180°C, 45 mins	118,0

Using the 8-fold parallel reactor provided by the BasCat laboratory, equipped with one oven and a single feed charge for all samples, an optimal comparability could be achieved. The catalysts were placed in quartz tube reactors, where the outlet could be constricted by inserting quartz rods to reducing the reactor volume. This was done in order to prevent gas phase reactions, resulting in the combustion of the products and therefore a reduced selectivity. The influence of the usage of the rods can be seen in figure 20.

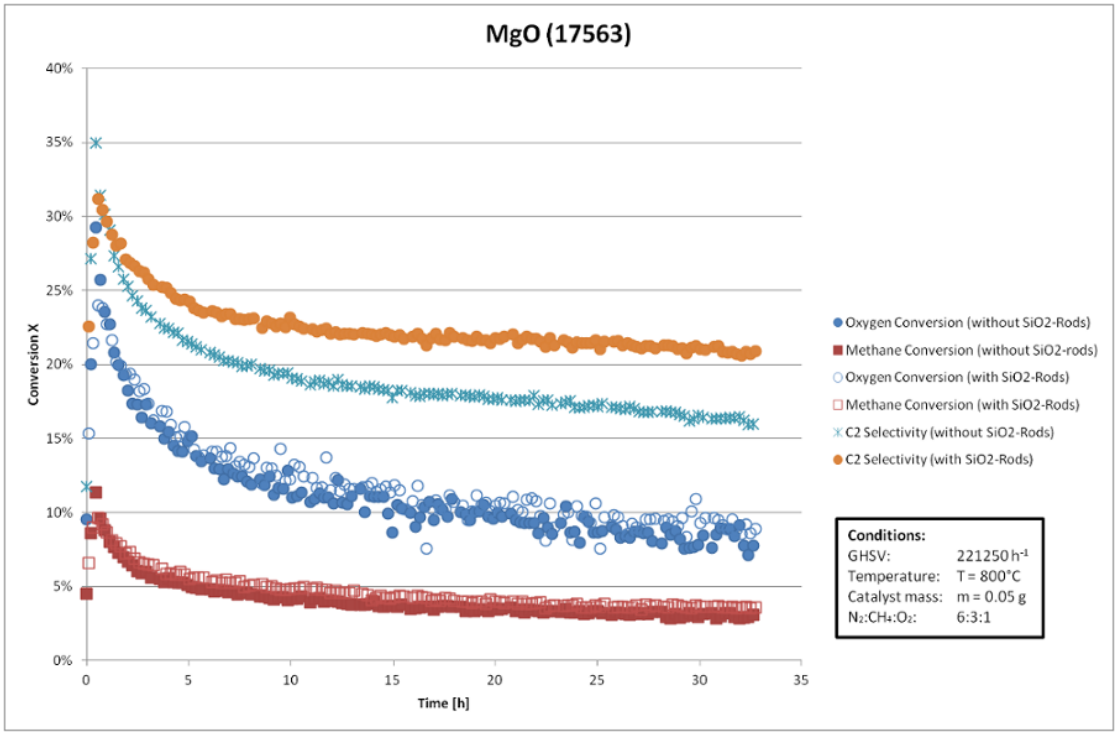

Figure 20: Effect of gas phase reaction during OCM, using quartz rods to reduce the outlet reactor volume.

It can be noted, that the insertion of the rods has no influence on the conversion, proving that there is no methane activation by gas phase reaction, the selectivity however is increased. The far more unstable reaction products react, even in absence of any catalyst, making reactor design an important subject in OCM research. Further experiments were conducted with reduced reactor outlet volume.

To compare both oxides under the same reaction conditions 50 mg catalyst material (d_r = 0,2-0,3 mm) were used, applying a GHSV of 47755 h^{-1}, with a feed composition N_2:CH_4:O_2 of 3:3:1, allowing to observe the activity of magnesium oxide without having full oxygen conversion at the calcium oxide catalysts. The catalysts were observed over a period 70 h with one reading point per hour per catalyst.

The conversions during of the catalytic tests are presented in figure 21. At first glance

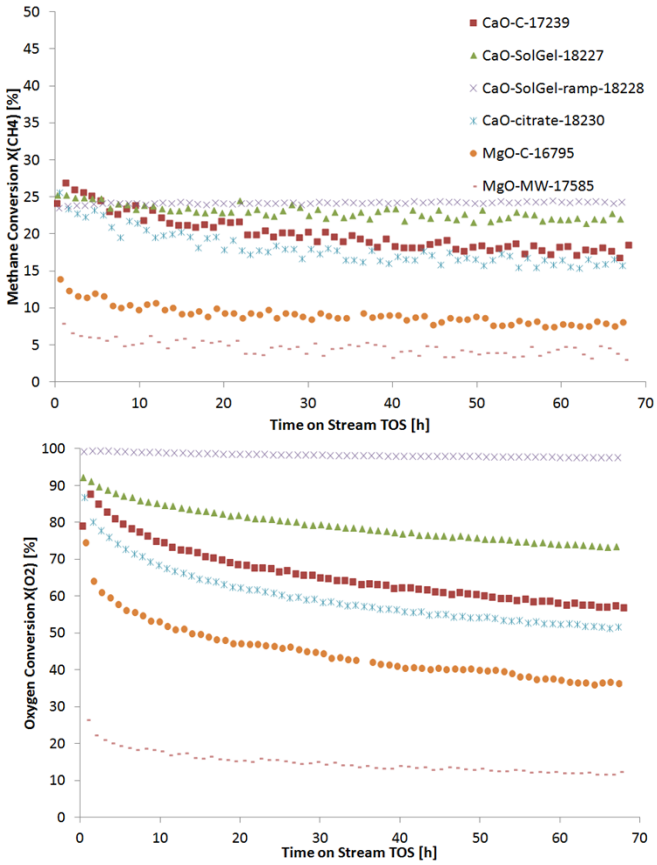

Figure 21: Methane (top) and Oxygen (bottom) conversion during OCM. 50 mg catalyst, GHSV 47755 h^{-1}, 750° C, N_2:CH_4:O_2 = 3:3:1.

it can be noticed, that the activity for calcium oxide samples are by a magnitude higher compared to magnesium oxide. For both oxides the conversion drops over the reaction time, indicating a sintering of all materials. The oxygen conversion for the calcium oxide

catalyst is to high to conduct established kinetic investigations. Decreasing the temperature or increasing the GHSV makes a comparison with magnesium oxide challenging due to the weak conversions. The highest conversions were achieved by the Ca-SolGel-ramp followed by the SolGel, the commercial and the citrate one. Among the MgO samples the raw commercial one achieved the better results. Given the low surface area of the commercial CaO one in comparison to the other CaO samples, it appears to have the highest activity. At the first measurement point all samples show a high initial activity which dropped pretty fast. After 60 hours on stream the methane conversion stabilises resulting in a conversion of maximal 25% for the SolGel-ramp and minimal of 18% for the commercial CaO. The magnesium oxide catalysts only achieved a methane conversion of 8% in case of C-MgO and 4% in case of MW-MgO after 60 hours on stream, while having significant higher surface area. In case of oxygen conversion with exception of the SolGel-ramp sample, all samples deactivate strongly during the testing.

The selectivity of the catalyst (figure 22) also shows higher values in for calcium oxide. After an initial drop in case of the C-CaO sample, the selectivity for all samples towards C_2 products appears to be quite stable around 30% for CaO and up to 12% for MgO. For the CaO-SolGel-ramp sample the selectivity is lower compared to the other calcium samples. A possible explanation for this might be the oxygen limitation causing a different pathway for the reaction at the catalyst surface. Examining the S-X plot, the highest yield can initially be achieved initially with the commercial CaO, before the decreased activity.

Using gradual CO-adsorption coupled with IR-investigation (cf. section 4.3), the surface of the calcium oxide samples was analysed (figure 23). The recorded isotherms show for each sample a unique adsorption pattern, what indicates divers surface site compositions. Due to the small surface area, the C-CaO sample is quickly saturated, what can be seen observing by the detection of vibrational frequencies of the CO molecule. All samples feature the three signals found in section 4.3, in which the distribution of the intensities vary strongly. Whereas the C-CaO appears to have a high amount of edge

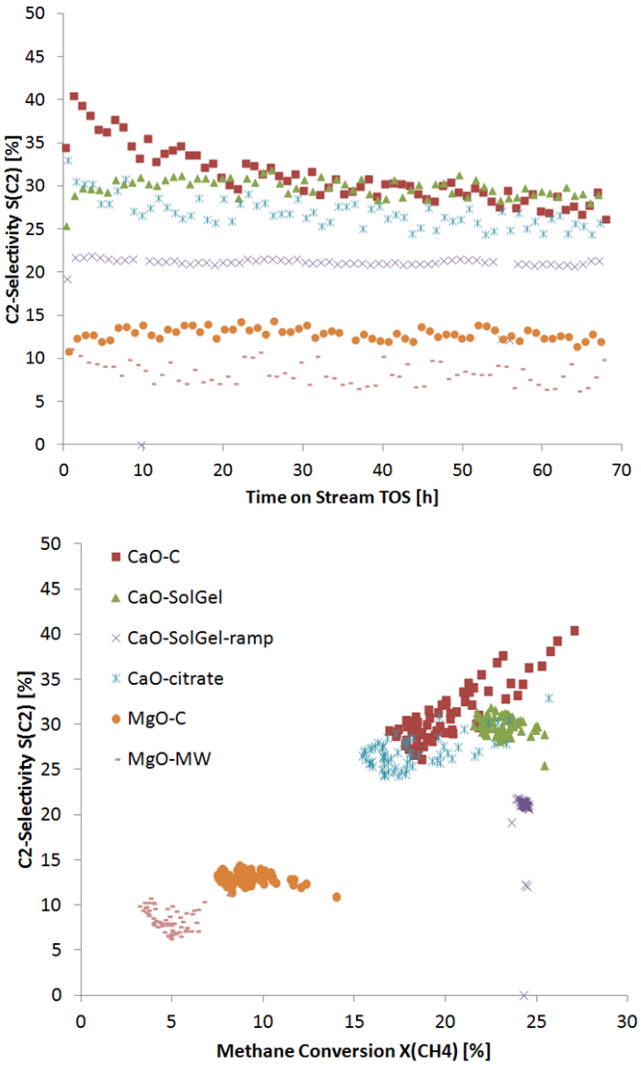

Figure 22: Selectivity (top) and S-X plot (bottom) during OCM. 50 mg catalyst, GHSV 47755 h^{-1}, 750° C, N_2:CH_4:O_2 = 3:3:1.

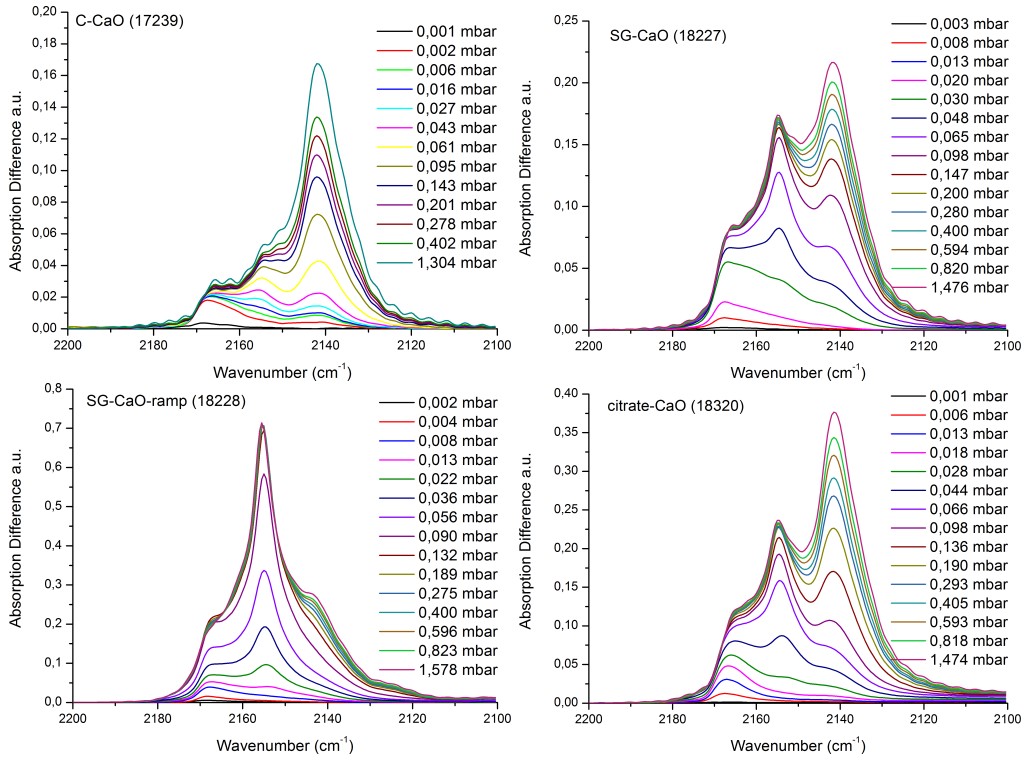

Figure 23: IR-investigation of CO adsorbed on calcium oxides used in OCM.

sites, represented by the band at 2164 cm^{-1}, the SolGel-ramp sample features a very sharp peak at 2154 cm^{-1} indicating a large amount of terrace sites.

To compare the measured spectra the carbonyl areas of the recorded spectra were integrated and a coverage was calculated (figure 24, cf. section 4.3). The spectra at a

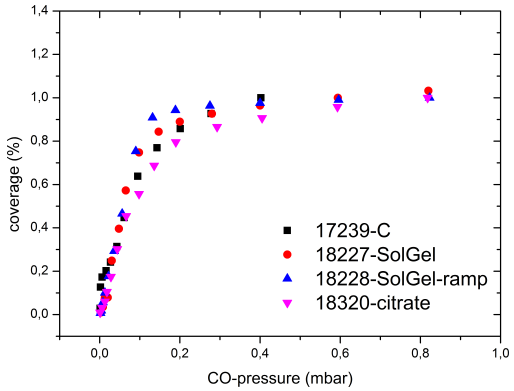

Figure 24: CO-coverage during adsorption experiment of CaO catalysts.

coverage of roughly 50% are presented in figure 25. By normalising the spectra by the highest peak the surface site composition can be discussed qualitatively.

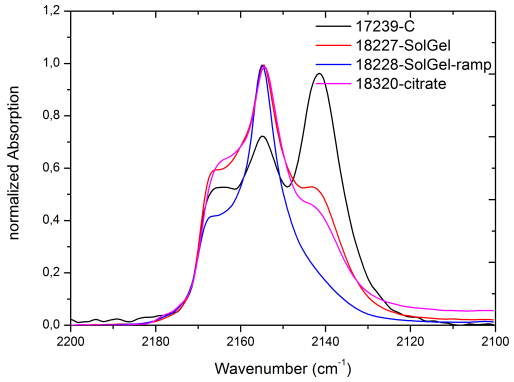

Figure 25: Normalised IR spectra of carbonyl area at roughly 50% coverage of CaO catalysts.

The highest peak for most of the samples is located at 2154 cm^{-1}, which was previously assigned to the CO adsorbed on terrace sites. In case of C-CaO sample the peak at

2141 cm^{-1}, which was assigned to physisorbed or free CO (cf. section 4.3), had the greatest height, indicating a full saturation instead of a 50% coverage. Nevertheless, under the assumption that the surface sites corresponding to the absorption at 2154 cm^{-1} and 2164 cm^{-1} are saturated, the peak height difference should give information on the surface composition. Under these assumptions the surface SolGel-ramp sample has highest amount of terrace sites, followed by SolGel and the citrate sample and the commercial sample with the least amount of terrace sites.

Adapting those results to the reaction behaviour discussed above and given that commercial CaO shows a high initial activity and selectivity, despite its low surface area, it can be assumed, that the edge sites on calcium oxide favour the oxidative coupling of methane for selectivity as well as reactivity. Due to the lower stability of the unsaturated coordination sites, those are also more likely to vanish during the reaction forming bigger terrace sites. This causes a strong decrease in the initial activity and selectivity, which is stronger pronounced by the commercial and the citrate CaO. The constant mediocre selectivity in case of the SolGel-ramp sample supports this assumption, showing the smallest concentration of edge sites. The higher activity of this sample can be attributed to the higher surface area. However, due to the high oxygen consumption, the mediocre selectivity might be the cause of kinetic effects.

After the initial drop of the activity, caused by the surface restructuring, the activity of samples constantly drops. In situ XRD (figure showed a particle size growth during the reaction. The volume weighted particle sizes calculated using TOPAS software (figure 26). Over a period of approximately 20 h the particle sizes increased by at least 20%, appearing this to be the deactivation process. Coking or forming of other phases could not be observed.

Having not undergone a calcination prior to the catalytic experiments, explains why the commercial samples for both MgO and CaO show higher initial catalytic performances. The calcination process for the other catalyst necessary to decompose the precursors

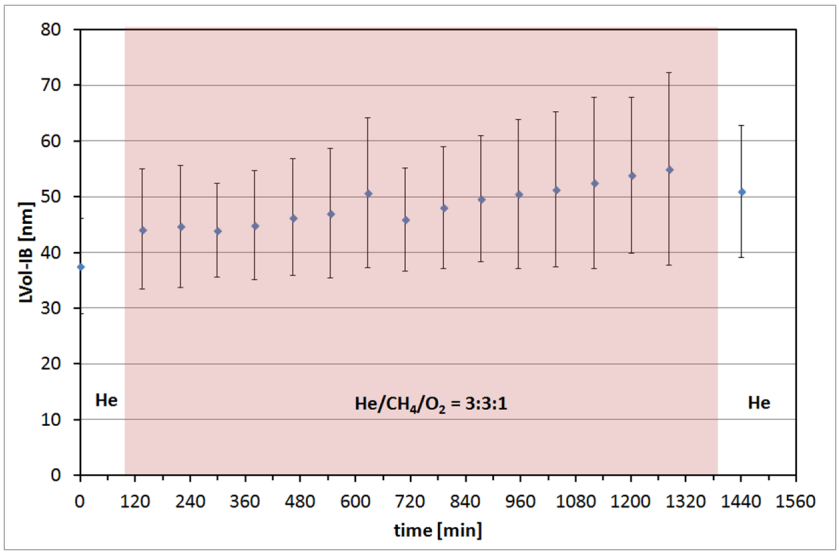

Figure 26: Particle size growth of calcium oxide (18228) during OCM reaction using in situ XRD. Gas feed composition He:CH_4:O_2 = 3:3:1.

during the synthesis, causes a sintering before the catalysis and more pristine structures.

In summary, the catalytic activity for calcium oxide can be explained by its surface properties. Unsaturated surface sites, such as edge sites, enhance activity as well as selectivity. The more saturated terrace sites show inferior catalytic activity. Compared to the two measured magnesium oxide samples, all calcium oxide samples exhibited higher conversions and selectivity, making it a more suitable material fur further investigations.

These results prove the importance of surface analysis for profound catalytic studies using calcium oxide and explain the differences in catalytic performance by calcium oxide catalysts of different origins reported in the literature.[16,17]

5 Conclusion

Among the applied synthetic procedures the Sol-Gel inspired method has proven to be the most promising to produce nanocrystalline calcium oxide with surface areas up to $40\,m^2/g$. Embedding of metal impurities can be reduced to a minimum by only using high quality calcium and organic solvents, making this method suitable to produce highly pure samples.

The conditions during the calcination strongly affect the size and surface of the resulting oxide. The presence of CO_2 and H_2O lead to larger particles and therefore smaller surface areas. Best results could be obtained by calcination under vacuum.

Microwave assisted hydrothermal treatment can be used to alter and increase the surface of given magnesium oxide and calcium oxide. The surface areas could be enhanced by a factor of two.

IR-investigations at 77 K on calcium oxide using CO as probe molecule show three different carbonyl species at $2164\,cm^{-1}$, $2154\,cm^{-1}$ and $2141\,cm^{-1}$, in which the last species appears to be physisorbed. Due to similarities between the adsorption patterns of calcium oxide and magnesium oxide, the species at $2164\,cm^{-1}$ was assigned to edge sites and the species at $2154\,cm^{-1}$ to terrace sites.

HR-TEM imaging proved the presence of monoatomic steps on the surface of both oxides.

Calcium oxide shows in contrast to magnesium oxide O-H terminations at the surface even after activation under vacuum at 1123 K, proving its stronger basic character.

The reactivity of calcium oxide in the OCM reaction is by a magnitude higher compared to magnesium oxide, making a comparison of both materials under the same reaction conditions difficult.

Reaction rate as well as selectivity for calcium oxide are higher than magnesium oxide,

making it better suitable as a benchmark material for future OCM research.

The sensitivity to the reaction products accelerates the sintering during the reaction, causing the reaction rate to constantly drop over the operation time.

Differences in rate and selectivity among the calcium oxide samples can be explained by the different surface site compositions of the samples, assuming edges to be favourable for a selective OCM.

6 Outlook

In further studies the Sol-Gel inspired synthesis can be improved, by attempting to remove all carbon components before calcination, to eliminate potential carbon embedding as carbonate or carbide. This might be achieved by hydrothermal or steam treatment.

The resulting oxide can be altered by microwave assisted hydrothermal treatment to create a family of catalyst for better comparability.

Further kinetic investigations need to be done to compare calcium oxide with magnesium oxide. Therefore optimal reaction conditions have to be found.

EPR experiments as well as theoretical studies can be performed to get information on micro kinetics.

CO-adsorption experiments using IR spectroscopy along with HR-TEM investigations have to be done to confirm the assignment of the observed peaks to the corresponding surface sites.

After understanding the pure calcium oxide, the catalyst can be doped to enhance the performance and attempts can be made to stabilise the catalyst.

7 Experimental

7.1 Catalyst Preparation

7.1.1 Hydrothermal Treatment (MW-)

Commercial (C-) MgO (Alfa Aesar, Puratronic®, 99,998%) was altered by hydrothermal treatment in microwave heated teflon pressure vessels (Berghof Products + Instruments GmbH, Speedwave MWS-3+). Therefore 3.3 g of MgO was suspended in 40 ml distilled water and heated in a 60 ml teflon vessel to 493 K for 45-180 minutes.

Alternatively a magnetic stirred microwave system (Anton Paar, Monowave 300) was used. In this case 1 g MgO and CaO (Alfa Aesar, Puratronic®, 99,998%) were each suspended in 15 ml water using 20 ml quartz pressure vessels. The suspensions were treated for 45 min at 453 K.

The products of each procedure were filtered and washed with distilled water and dried at 383 K for at least 12 h giving the precursor of MW-oxides.

7.1.2 CaO Synthesis

7.1.2.1 Precipitation Method

For this method a 0.5 M solution of 3.3 g calcium nitrate hydrate (Roth, ROTI®METIC, 99,999%), 40 g water and a 0.7 M NaOH solution of 1,3 g sodium hydroxide monohydrate (Merck, Suprapur®, 99,99%) in 40 g water were mixed under vigorous stirring and stirred for another 10 min. The solution was afterwards equally distributed to three Berghof microwave vessels (see 7.1.1) and heated for 15 min at 473 K. The products were unified, filtered and washed with distilled water and ethanol and then dried at 383 K for at least 12 h.

7.1.2.2 Citrate Method (citrate-)

6.6 g calcium nitrate hydrate (Roth, ROTI®METIC, 99,999%) and 8.6 g citric acid (Alfa Aesar, 99+%) were solved in 28.7 g water, which under stirring was slowly evaporated at 353 K until a high viscous yellow gel was formed. The gel was dried at 383 K and 200 mbar for at least 12 h giving the precursor for citrate-CaO.

7.1.2.3 Sol-Gel Method (SG-)

Using a wire cutter 1.0 g metallic calcium (Sigma Aldrich, dendritic, 99,99%) was cut inside a glovebox into small pieces and transferred to a three neck round bottom flask. Under stirring in nitrogen atmosphere 24.9 g methanol (Sigma Aldrich, 99,8%) was added. The reaction mixture was heated to 323 K to accelerate the reaction. The resulting suspension was stirred for at least 12 h. After the total conversion of the metallic calcium, 158,8 g toluene was added and the suspension was stirred for another 24 h. In the next step 1,2 ml distilled water was added drop-wise to the suspension followed by another 24 h of stirring.

80 g of the suspension was transferred into the glass liner of a 300 ml stainless steel Parr autoclave. The system was purged with nitrogen and pressurised to 7 bar. The suspension was heated under stirring to 538 K over a period of at least 4 h. The system was allowed to equilibrate for 10 min giving a final pressure of 40 bar. The stirrer and heater were turned off and the pressure was released over a period of 10 min causing the temperature to drop to 493 K. The resulting solid was used as precursor for SG-CaO.

7.1.3 Calcination Process

Each of the used syntheses methods results in decomposable precursors consisting of hydroxides or organic compounds. The precursors were placed in a quartz crucible and calcined in synthetic air $Ar:O_2 = 4:1$ (except for sample 18115, which was calcined under dynamic vacuum $5 \cdot 10^{-2}$mbar) using a tube furnace applying a flow of 100 ml/min. The

samples were heated to up to 1123 K for 6 h applying a heating rate of 5 K/min.

In case of the Sol-Gel method some samples (17967, 18115 and 18228) were calcined using a temperature ramp. According to the measured thermo gravimetric analysis (figure 10) those samples were kept at 673 K for 3 h and 873 K for 3 h before heating to the final temperature.

For XRD and EM investigations the samples needed to be transferred into a glove-box to prevent exposure to H_2O and CO_2.

7.2 Analysis

7.2.1 IR-Measurement

The IR spectra were recorded with a Perkin-Elmer Spectrum 100 system equipped with a MCT detector. Scanning the range from 4000 cm^{-1} to 900 cm^{-1} (the usage of CaF windows making scans below 900 cm^{-1} obnoxious) in transmission mode the resolution was set to 2 cm^{-1} with an accumulation of 128 scans.

To conduct the measurements, the samples were pressed to wafers applying a pressure of approximately 123 MPa. The wafers were transferred into a gold holder and introduced into the IR set-up. The set-up is connected to a vacuum system reaching a residual pressure of up to 10^{-7} mbar. An attached oven was used to heat the samples to 1123 K for 6 h applying a heating rate of 5 K/min under dynamic vacuum prior to the experiments, converting hydroxides and carbonates to the desired oxide.

For the CO-adsorption experiments, the samples were indirectly cooled to approximately 77 K using a pumping system with liquid nitrogen. To ensure a heat transfer 2 mbar He were introduced. After reaching a constant temperature measurements were conducted. The CO (99,999%, Messer) could be dosed using a manual valve. The time between dosing and start of the measurement has been kept constant at 2 min, to keep a potential

error of the adsorption kinetics constant. The equilibrium pressure after the measurement was noted for the particular experiment. After the last experiment the chamber was evacuated to verify the reversibility of the adsorption.

7.2.2 Electron Microscopy

Morphological SEM studies were performed using a Hitachi S-4800 field emission scanning electron microscope. The samples were immobilised on an aluminium sample holder using carbon tape. The "low" resolution TEM images were recorded with a Phillips CM200 FEG. High resolution (HR) TEM images were recorded using FEI Titan 80-300 Cs-corrected microscope. The samples were prepared dry most of the time.

7.2.3 Nitrogen Adsorption

The surface area determination was performed using an AUTOSORB-6B analyser by Quantachrome. A 11-point analysis was performed, adsorbing nitrogen at 77K. The surface area was calculated using the BET-method. Prior to adsorption, the samples were degassed at 473 K (623 K for the samples mentioned in table 3) for 2 h.

7.2.4 TG-Analysis

For thermograviteric analysis a STA 449 C Jupiter thermo-microbalance by Netzsch was used. Exhaust gases were analysed with a QMS 200 mass spectrometer by Pfeiffer. For analysis the samples were heated in 100 ml/min Ar or synthetic air applying a heating rate of 5 K/min.

7.2.5 XRD-Analysis

X-ray diffraction was carried out with a Bruker AXS D8 ADVANCE diffractometer using the Bragg-Bretano reflection geometry. The diffractometer uses Cu $K_{\alpha 1}$ radiation. The powder is placed in a sample holder and flattened. The diffraction patterns were recorded in a 2Θ range between 20°to 90°.

For in situ XRD the sample was activated at 1023 K in a synthetic air stream of 100 ml/min (He:O_2 4:1). The first measurement was conducted at the final temperature, while switching the gas feed to 100% helium to flush out the oxygen. The gas feed was set to reaction conditions (He:CH_4:O_2 3:3:1) for 20 h. For particle size determination the patterns were fitted using the TOPAS software using the volume-weighted crystallite size distribution.

7.3 Catalytic Testing

For the catalytical tests an 8-fold parallel reactor (figure 27) from ILS-Integrated Lab Solutions was used, allowing simultaneous measurements of all catalysts under the same conditions. The feed gases were dosed and mixed using Bronckhorst mass-flow controller, and equally divided on 8 reactors plus one bypass stream using fitted capillaries. The used gases were provided by air liquide with a quality of Alphagaz^{TM} 1 or above. The quartz reactors (inner diameter of 4 mm and outer diameter of 6 mm) were placed in a sintered SiC oven, having an isothermal zone of 100 mm.

The exhaust gas was analysed using Agilent 7890A GC equipped with one FID for combustible and two TCD-detectors for incombustible products, analysing C_1 to C_4 products. With a full analysis time of 6 min the resolution of the measurement is one per hour for each reactor.

For the tests 50 mg catalysts (size 0,2-0,3 mm) resulting in a bed length of 5 mm were

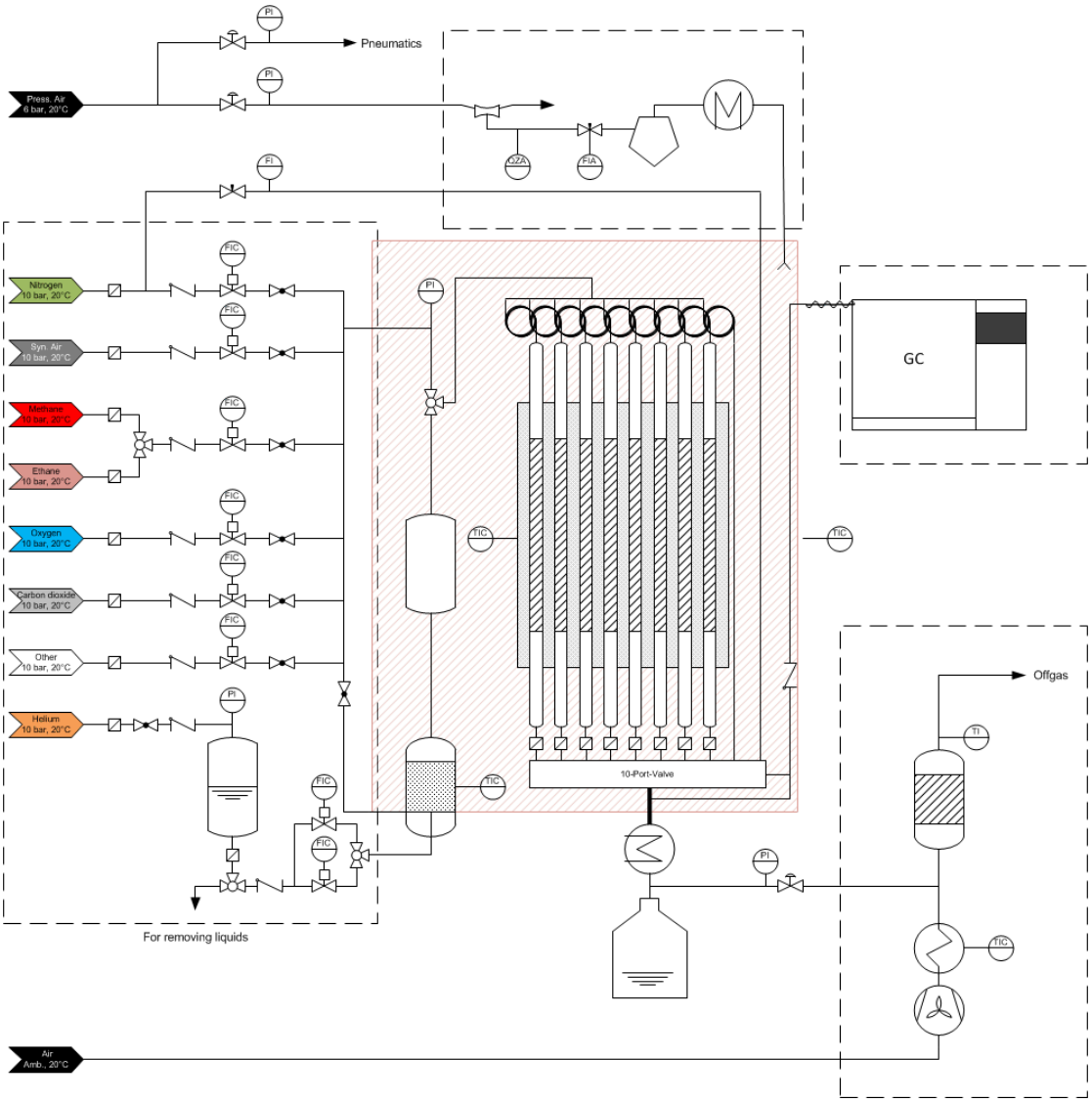

Figure 27: Scheme of 8-fold parallel reactor for catalytic testing (BasCat Laboratory).

used. To ensure the criteria for the plug flow model:

$$\frac{L}{d_P} > 50, \quad \frac{d_r}{d_P} > 10, \text{ and } \quad \frac{L}{d_r} > 5$$

with L the catalytic bed length, d_r the reactor diameter and d_P the particle diameter, SiC (size 0,3-0,4 mm) was placed above the catalytic bed, resulting in a full de length of 400 mm. The catalysts were fixed by quartz wool. To constrict the volume of the reactors at the outlet, quartz rods could be placed below the catalytic bed.

Before reaching the testing temperature of 1023 K with a heating rate of 10 K/min, synthetic air was used to activate the catalyst. After reaching the target temperature the feed was switched to 3:3:1 N_2:CH_4:O_2 applying a GHSV of 47755 h^{-1}.

The measured concentrations of the bypass stream were used as internal standard to correct fluctuations in the feed stream and volume effects.

The calculation of the oxygen conversion was calculated by:

$$X_{O_2} = \frac{O_{2,Bypass} - \frac{N_{2,Bypass}}{N_2} \cdot O_2}{O_{2,Bypass}},$$

methane conversion by:

$$X_{C_4} = \frac{CH_{4,Bypass} - \frac{N_{2,Bypass}}{N_2} \cdot CH_{4,Bypass}}{CH_{4,Bypass}},$$

and C2-selectivity by:

$$S_{C_2} = \frac{\frac{N_{2,Bypass}}{N_2} \cdot 2 \cdot \sum C_{2,Products}}{X_{CH_4} \cdot CH_{4,Bypass}}.$$

The mass balance of carbon was determined by subtracting the sum of all analysed carbon products multiplied with the number of carbon atoms per molecule from the methane inlet. The balance was acceptable at 100% ± 1,5%.

List of Figures

Bibliography

[1] Schwach, P.; Hamilton, N.; Frandsen, W.; Willinger, M.; Schlögl, R.; Trunschke, A. *unpublished* **2013**,

[2] Schwach, P.; Willinger, M. G.; Trunschke, A.; Schlögl, R. *Angewandte Chemie International Edition* **2013**, *52*, 11381–4.

[3] Otsuka, K.; Jinno, K.; Morikawa, A. *Chem. Lett.* **1985**, *4*, 499–500.

[4] Cui, Y.; Shao, X.; Baldofski, M.; Sauer, J.; Nilius, N.; Freund, H. *Angewandte Chemie (International ed. in English)* **2013**, *52*, 11385–11387.

[5] Keller, G.; Bhasin, M. *J. Catal.* **1982**, *73*, 9–19.

[6] BP, BP Statistical Review of World Energy. 2014; `bp.com/satisticalreview`.

[7] Baerns, M.; Behr, A.; Brehm, A.; Gmehling, J.; Hofmann, H.; Onken, U. *Technische Chemie*; Wiley-VHC, 2006; pp 534–541.

[8] Shuichi, N. *Catalysis Surveys from Japan* **2000**, *4*, 3–15.

[9] Zavyalova, U.; Holena, M.; Schlögl, R.; Baerns, M. *ChemCatChem* **2011**, *3*, 1935–1947.

[10] Ito, T.; Ji-Xiang, W.; Chiu-Hsun, L.; Lunsford, J. H. *J. Am. Chem. Soc.* **1985**, *107*, 5062–5068.

[11] Arndt, S.; Simon, U.; Heitz, S.; Berthold, A.; Beck, B.; Görke, O.; Epping, J. D.; Otremba, T.; Aksu, Y.; Irran, E.; Laugel, G.; Driess, M.; Schubert, H.; Schomäcker, R. *Top. Catal.* **2011**, *54*, 1266–1285.

[12] Zavyalova, U.; Geske, M.; Horn, R.; Weinberg, G.; Frandsen, W.; Schuster, M.; Schlögl, R. *ChemCatChem* **2011**, *3*, 949–959.

[13] Zhanpeisov, N. U.; Staemmler, V.; Baerns, M. *J. Mol. Catal. A: Chem.* **1995**, *101*, 51–60.

[14] Sun, X.; Li, B.; Metiu, H. *The Journal of Physical Chemistry C* **2013**, *117*, 7114–7122.

[15] Yamagata, N.; Tanaka, K.; Sasaki, S.; Okazaki, S. *Chem. Lett.* **1987**, *16*.

[16] Carreiro, J. A. S. P.; Baerns, M. *J. Catal.* **1989**, *117*, 258–265.

[17] Carreiro, J. A. S. P.; Baerns, M. *J. Catal.* **1989**, *117*, 396–403.

[18] Holleman, A.; Wiberg, E.; Wiberg, N. *Lehrbuch der Anorganischen Chemie*; deGuyter, 2007; pp 1938–1940.

[19] Lin, C. H.; Ito, T.; Wang, J.; Lunsford, J. H. *J. Am. Chem. Soc.* **1987**, *109*, 4808–4810.

[20] Choudhary, V. R.; Rane, V. H.; Chaudhari, S. T. *Applied Catalysis A: General* **1997**, *158*, 121–136.

[21] Rane, V. H.; Chaudhari, S. T.; Choudhary, V. R. *Journal of Chemical Technology & Biotechnology* **2006**, *81*, 208–215.

[22] Rane, V.; Chaudhari, S.; Choudhary, V. *J. Nat. Gas Chem.* **2008**, *17*, 313–320.

[23] Rane, V. H.; Chaudhari, S. T.; Choudhary, V. R. *J. Nat. Gas Chem.* **2010**, *19*, 25–30.

[24] Arndt, S.; Laugel, G.; Levchenko, S.; Horn, R.; Baerns, M.; Scheffler, M.; Schlögl, R.; Schomäcker, R. *Catalysis Reviews* **2011**, *53*, 424–514.

[25] DeBoy, J. M.; Hicks, R. F. *Applied Catalysis* **1988**, *27*, 1577–1582.

[26] Moriyama, T.; Takasaki, E., N. Iwamatsu; Aika, K.-I. *Chem. Lett.* **1986**, *15*, 1168–

1168.

[27] Hu, Z.; Li, B.; Sun, X.; Metiu, H. *J. Phys. Chem. C* **2011**, *115*, 3065–3074.

[28] An, B.-i.; Ryu, K.-h.; Kim, Y.-r.; Lee, S.-h. *Bull. Korean Chem. Soc.* **2007**, *28*, 1049–1052.

[29] Nakamura, M.; Mitsuhashi, H.; Takezawa, N. *J. Catal.* **1992**, *138*, 686–693.

[30] Satsuma, A.; Akahori, R.; Kato, M.; Yoshida, H.; Hattori, T. *J. Mol. Catal. A: Chem.* **2000**, *155*, 81–88.

[31] Zhu, Y.; Wu, S.; Wang, X. *Chemical Engineering Journal* **2011**, *175*, 512–518.

[32] Borgwardt, R. H. *Ind. Eng. Chem. Res.* **1989**, *28*, 493–500.

[33] Hofmann, P.; Knözinger, E.; Diwald, O.; Mustafa, A. *Ber. Bunsenges. Phys. Chem.* **1997**, *11*, 1722–1725.

[34] Müller, M.; Sternig, A.; Stankic, S.; Sto, M.; Bernardi, J.; Kno, E.; Diwald, O. *The Journal of Physical Chemistry C* **2008**, *112*, 9120–9123.

[35] Spoto, G.; Gribov, E.; Ricchiardi, G.; Damin, a.; Scarano, D.; Bordiga, S.; Lamberti, C.; Zecchina, a. *Prog. Surf. Sci.* **2004**, *76*, 71–146.

[36] Babaeva, M.; Bystrov, D.; Kovalgin, A.; Tsyganenko, A. *J. Catal.* **1990**, *123*, 396–416.

[37] Roy, A.; Bhattacharya, J. *Int. J. Nanosci.* **2011**, *10*, 413–418.

[38] Luo, C.; Zheng, Y.; Ding, N.; Wu, Q. L.; Zheng, C. G. *Chin. Chem. Lett.* **2011**, *22*, 615–618.

[39] Santos, E.; Alfonsín, C.; Chambel, A.; Fernandes, A.; Soares Dias, A.; Pinheiro, C.; Ribeiro, M. *Fuel* **2012**, *94*, 624–628.

[40] Koper, O. B.; Lagadic, I.; Volodin, A.; Klabunde, K. J. *Chem. Mater.* **1997**, *9*, 2468–2480.

[41] Yingli, B.; Kaiji, Z.; Yutao, J.; Chiwen, T.; Xiangguong, Y. *Ind. Eng. Chem. Res.* **1988**, *27*, 1577.

[42] Koper, O.; Li, Y. X.; Klabunde, K. J. *Chem. Mater.* **1993**, *5*, 500–505.

[43] Liu, C.; Zhang, L.; Deng, J.; Mu, Q.; Dai, H.; He, H. *The Journal of Physical Chemistry C* **2008**, *112*, 19248–19256.

[44] Klabunde, K. J.; Stark, J.; Koper, O.; Mohs, C.; Park, D. G.; Decker, S.; Jiang, Y.; Lagadic, I.; Zhang, D. *J. Phys. Chem.* **1996**, *3654*, 12142–12153.

[45] Hadjiivanov, K. I.; Vayssilov, G. N. *Adv. Catal.* **2002**, *47*, 307–511.

[46] Spoto, G.; Gribov, E.; Damin, A.; Ricchiardi, G.; Zecchina, A. *Surf. Sci.* **2003**, *540*, L605–L610.

[47] Trionfetti, C.; Babich, I.; Seshan, K.; Lefferts, L. *Langmuir* **2008**, *24*, 8220.